The Stability of Hotspots for a Reaction-Diffusion Model of Urban Crime with Focused Police Patrol

Wang Hung Tse* , Michael J. Ward†

November 21, 2017

Abstract

1 Introduction

In this chapter, we consider the simple interaction case for the police-criminal dynamics ($I(\rho, U) = U$) in the three-component reaction-diffusion model. The following model is included as a special case of a general form proposed in [26]. In particular, the simple interaction term $-U$ in the ρ-equation (criminal density) represents a criminal removal rate proportional to the number of police present at the same spatial location. The nonlinear police movement term corresponds to a choice of the function $v(A)$ not explicitly studied in [26], given by

$$v(A) = qD\nabla \log A\,.$$

Our simple police interaction model on the one-dimensional domain $0 \le x \le S$ is formulated as

$$A_t = \epsilon^2 A_{xx} - A + \rho A^3 + \alpha\,, \tag{1.1a}$$

$$\rho_t = D\left(\rho_x - 2\rho A_x/A\right)_x - \rho A + \gamma - \alpha - U\,, \tag{1.1b}$$

$$\tau_u U_t = D\left(U_x - qUA_x/A\right)_x\,, \tag{1.1c}$$

where $A_x = \rho_x = U_x = 0$ at $x = 0, S$. By integrating (1.1c) over the domain, we obtain that the total level U_0 of police deployment is conserved in time, so that

$$U_0 \equiv \int_0^S U(x,t)\,dx\,. \tag{1.2}$$

In (1.1c), the parameter $q > 0$ measures the degree of focus in the police patrol toward maxima of the attractiveness field A. We will assume in our analysis below that $q > 1$. The choice $q = 2$ models a "cops-on-the-dots" strategy (cf. [12], [26], [38]) whereby the police have the same degree of focus as do the criminals towards maxima of A. When q is above or below 2, the police force drift in a less or more focused manner, respectively, as compared to the movement of the criminals. In (1.1c), the "diffusivity" of the police is D/τ_u, so that when $\tau_u < 1$, the police are more mobile than the criminals. Conversely, $\tau_u > 1$ corresponds to the police being comparatively more "sluggish" in their movements than the criminals.

*Dept. of Mathematics, UBC, Vancouver, Canada
†Dept. of Mathematics, UBC, Vancouver, Canada. (corresponding author ward@math.ubc.ca)

For the analysis, it is convenient to introduce the new variables (cf. [14])

$$\rho = VA^2\,, \qquad U = uA^q\,, \tag{1.3}$$

so that (1.1) transforms to

$$A_t = \epsilon^2 A_{xx} - A + VA^3 + \alpha\,, \tag{1.4a}$$

$$\left(VA^2\right)_t = D\left(A^2 V_x\right)_x - VA + \gamma - \alpha - uA^q\,, \tag{1.4b}$$

$$\tau_u\left(uA^q\right)_t = D\left(A^q u_x\right)_x\,. \tag{1.4c}$$

When $\epsilon \ll 1$ the attractiveness field A is spatially localized. For the diffusivity D, we consider the regime $D = \mathcal{O}(\epsilon^{-2})$ where steady-state hotspot patterns were found to have a stability threshold for the basic crime model (cf. [14]). For this regime in D, we take $V = \mathcal{O}(\epsilon^2)$ to obtain a distinguished balance (cf. [14]). This motivates the rescaling

$$V = \epsilon^2 v\,, \qquad D = \epsilon^{-2}\mathcal{D}_0\,, \tag{1.5}$$

so that in terms of v and $\mathcal{D}_0 = \mathcal{O}(1)$, (1.4) becomes

$$A_t = \epsilon^2 A_{xx} - A + \epsilon^2 vA^3 + \alpha\,, \tag{1.6a}$$

$$\epsilon^2\left(A^2 v\right)_t = \mathcal{D}_0\left(A^2 v_x\right)_x - \epsilon^2 vA^3 + \gamma - \alpha - uA^q\,, \tag{1.6b}$$

$$\tau_u\epsilon^2\left(A^q u\right)_t = \mathcal{D}_0\left(A^q u_x\right)_x\,. \tag{1.6c}$$

One key issue that we will study for (1.6) is to determine whether there is an optimum degree of focus in the patrolling so as to reduce the number of possible crime hotspots in a given 1D spatial region. More specifically, we will investigate whether there are optimal values of q and τ_u so as to obtain the fewest number of stable steady-state hotspots on a given domain length. In mathematical terms, we will determine how the stability threshold in the diffusivity D for steady-state hotspot patterns depends on q, the police diffusivity D/τ_u, and the total level U_0 of police deployment.

To analyze the linear stability of a K-hotspot steady-state solution, in §3 we use asymptotic analysis to derive the nonlocal eigenvalue problem (NLEP), characterizing $\mathcal{O}(1)$ time-scale instabilities of the pattern. The methodology to derive this NLEP involves using a reference domain $|x| \le \ell$ containing a single hotspot centered at $x = 0$, and then imposing Floquet-type boundary conditions at $x = \pm\ell$. In terms of this reference problem, the NLEP for the finite-domain problem $0 < x < S$ with Neumann conditions at $x = 0, S$ can then readily be extracted, as similar to that done in [14] for the basic two-component crime model. Such a Floquet-based approach to study the linear stability of multi-spike steady-states was first introduced in [22] in the context of 1D spatially-periodic spike patterns for a class of two-component reaction-diffusion systems. It has subsequently been extended to study the linear stability of 1D mesa patterns [15], of 1D spikes for a competition model with cross-diffusion effects [17], and 1D hotspot patterns for the basic crime model [14]. There are two novel features in the derivation of the NLEP for our three-component RD system with police. Firstly, in our asymptotic analysis, we must carefully derive rather intricate jump conditions across the hotspot region. Secondly, the resulting NLEP that we obtain has two nonlocal terms, instead of one. As a result, its analysis is seemingly beyond the general NLEP stability theory with a single nonlocal term, as surveyed in [36]. However, by using some key identities that are particular to our three-component RD crime model, we show how to reformulate the NLEP more conveniently in terms of a single nonlocal term, which can then be more readily analyzed.

In §5 we show for the special case where $q = 3$ that the spectrum of the NLEP can be reduced to the study of a simple algebraic equation for the eigenvalue parameter. More specifically, we show that the problem of determining unstable eigenvalues of the NLEP reduces to determining roots λ in $\mathrm{Re}(\lambda) > 0$ to a quadratic equation. By analyzing this simple spectral problem for $q = 3$, we show explicitly that, when D is below a certain competition instability threshold, a spatial pattern of two hotspots can be destabilized by an asynchronous, or anti-phase, temporal oscillation in the hotspot amplitudes when the police diffusivity D/τ_u falls below a Hopf bifurcation value. This Hopf bifurcation threshold can be determined analytically. The existence of such robust asynchronous temporal oscillations in the hotspot amplitudes is a qualitatively new phenomena, which does not occur in the study of spike stability for other RD systems such as the Gierer-Meinhardt and Gray-Scott models. For these two-component models, previous NLEP stability analyzes have shown that the dominant oscillatory instability of the spike amplitudes is always a synchronous instability.

2 Asymptotic Construction of a Multiple Hotspot Steady-State

In this section we construct a steady-state solution to (1.6) on $0 \le x \le S$ with $K \ge 1$ interior hotspots.

To construct a symmetric steady-state with K interior hotspots to (1.6) on $0 < x < S$, we will first construct a one-hotspot solution to (1.6) on $|x| \le l$ centered at $x = 0$. Then, by using the translation-invariance property of (1.6), we obtain a K interior hotspot steady-state solution on the original domain of length $S = (2\ell)K$. In terms of this reference domain $|x| \le \ell$, (1.2) yields that

$$U_0 = K \int_{-\ell}^{\ell} U \, dx \,. \tag{2.1}$$

In this way, we need only construct a one-hotspot steady-state solution to (1.6) centered at $x = 0$ and impose $A_x = v_x = u_x = 0$ at $x = \pm\ell$. We refer to this as the *canonical* hotspot problem.

From the steady-state of (1.6c), together with $U = uA^q$ and (2.1), it follows that u is spatially constant and given by

$$u = \frac{U_0}{K \int_{-\ell}^{\ell} A^q \, dx} \,. \tag{2.2}$$

By using (2.2) in (1.6), the steady-state problem for the three-component system reduces to the following two-component system with a nonlocal term:

$$\epsilon^2 A_{xx} - A + \epsilon^2 v A^3 + \alpha = 0 \,, \qquad |x| \le \ell \,; \qquad A_x = 0 \quad x = \pm\ell \,, \tag{2.3a}$$

$$\mathcal{D}_0 \left(A^2 v_x \right)_x - \epsilon^2 v A^3 + \gamma - \alpha - \frac{U_0}{K} \frac{A^q}{\int_{-\ell}^{\ell} A^q \, dx} = 0 \,, \qquad |x| \le \ell \,; \qquad v_x = 0 \quad x = \pm\ell \,. \tag{2.3b}$$

We now construct the solution to (2.3) with a single hotspot centered at $x = 0$. In the outer region we have $A \sim \alpha + \mathcal{O}(\epsilon^2)$, while in the inner region we put $y = \epsilon^{-1} x$ and $A \sim A_0/\epsilon$ to obtain on $-\infty < y < \infty$ that

$$A_{0yy} - A_0 + v A_0^3 + \epsilon\alpha = 0 \,, \qquad \mathcal{D}_0 \epsilon^{-4} \left(A_0^2 v_y \right)_y + \mathcal{O}(\epsilon^{-1}) = 0 \,.$$

Therefore, to leading order it follows that $v \sim v_0$ is a constant, and that

$$A_0 \sim \frac{w(y)}{\sqrt{v_0}} \,, \tag{2.4}$$

where $w(y) = \sqrt{2}\,\mathrm{sech}\, y$ is the homoclinic solution of

$$w'' - w + w^3 = 0 \,, \qquad -\infty < y < \infty \,; \qquad w(0) > 0 \,, \quad w'(0) = 0 \,, \quad w \to 0 \quad \text{as} \quad y \to \pm\infty \,. \tag{2.5}$$

The integrals of $w(y)$ that are needed below are

$$\int_{-\infty}^{\infty} w\,dy = \int_{-\infty}^{\infty} w^3\,dy = \sqrt{2}\pi\,, \quad \int_{-\infty}^{\infty} w^2\,dy = 4\,, \quad \int_{-\infty}^{\infty} w^4\,dy = \frac{16}{3}\,, \quad \frac{\int_{-\infty}^{\infty} w^5\,dy}{\int_{-\infty}^{\infty} w^3\,dy} = \frac{3}{2}\,. \tag{2.6}$$

More generally, we can readily calculate in terms of the usual Gamma function $\Gamma(z)$ that

$$I_q \equiv \int_{-\infty}^{\infty} w^q\,dy = 2^{3q/2-1}\,\frac{[\Gamma(q/2)]^2}{\Gamma(q)}\,. \tag{2.7}$$

We return to (2.2), and for $q > 1$ we estimate the key integral

$$\int_{-\ell}^{\ell} A^q\,dx \sim 2\ell\alpha + \epsilon^{1-q} v_0^{-q/2} \int_{-\infty}^{\infty} w^q\,dy = \mathcal{O}(\epsilon^{1-q}) \gg 1\,.$$

From (2.2), it follows that $u = \mathcal{O}(\epsilon^{q-1}) \ll 1$ since $q > 1$. With our assumption $q > 1$, the integral $\int_{-\ell}^{\ell} A^q\,dx$, and thus u, depend to leading-order only on the inner region contribution from A^q. For $q > 1$, we obtain to leading-order from (2.2) that

$$u \sim \epsilon^{q-1}\tilde{u}_e\,, \qquad \text{where} \qquad \tilde{u}_e \equiv \frac{U_0 v_0^{q/2}}{K I_q}\,. \tag{2.8}$$

Next, we determine v_0 by integrating (2.3b) on $-\ell < x < \ell$ and then imposing $v_x(\pm\ell) = 0$. This yields that

$$\epsilon^2 \int_{-\ell}^{\ell} v A^3\,dx = 2\ell\,(\gamma - \alpha) - U_0/K\,.$$

Therefore, since $A \sim \alpha = \mathcal{O}(1)$ in the outer region, while $A = \mathcal{O}(\epsilon^{-1})$ in the inner region, it follows that, when $q > 1$, the dominant contribution to the integral arises from the inner region where $v \sim v_0$. In this way, we estimate

$$\frac{\int_{-\infty}^{\infty} w^3\,dy}{\sqrt{v_0}} = 2\ell\,(\gamma - \alpha) - U_0/K\,. \tag{2.9}$$

From (2.9), a steady-state hotspot solution exists only when the total level U_0 of police deployment is below a threshold given by

$$U_0 < U_{0,max} \equiv 2\ell K\,(\gamma - \alpha) = S(\gamma - \alpha)\,. \tag{2.10}$$

Here $S = 2\ell K$ is the original domain length. We will assume that (2.10) holds, so that a K-hotspot steady-state exists.

Upon solving (2.9) for v_0, and using (2.6) for $\int_{-\infty}^{\infty} w^3\,dy$, we get

$$v_0 = 2\pi^2\,[2\ell\,(\gamma - \alpha) - U_0/K]^{-2} = 2\pi^2 K^2\,[S(\gamma - \alpha) - U_0]^{-2}\,. \tag{2.11}$$

Since v_0 increases when either K increases or the total level U_0 of police increases, it follows from (2.4) that the maximum $A_{\max} \equiv A(0)$ of the attractiveness field, given by

$$A_{\max} \equiv A(0) \sim \epsilon^{-1} A_0(0) = \frac{\epsilon^{-1}}{\pi K}\,[S(\gamma - \alpha) - U_0]\,, \tag{2.12}$$

decreases with increasing K or increasing police deployment U_0. However, this maximum value of A is independent of the police patrol focus parameter q.

To complete the asymptotic construction of the hotspot, we must determine v. In the outer region, we expand $v \sim v_e(x) + \ldots$ and recall that $A \sim \alpha + \mathcal{O}(\epsilon^2)$ so that $A^q / \int_{-\ell}^{\ell} A^q\,dx = \mathcal{O}(\varepsilon^{q-1}) \ll 1$ since $q > 1$. In this way, from (2.3b), we obtain to leading order that $v_e(x)$ satisfies

$$\mathcal{D}_0 v_{exx} = -\frac{(\gamma - \alpha)}{\alpha^2}\,, \quad -\ell < x < \ell\,; \qquad v_e(0) = v_0\,, \qquad v_{ex}(\pm\ell) = 0\,. \tag{2.13}$$

The solution to (2.13) is

$$v_e(x) = \frac{\zeta}{2}\left[(\ell - |x|)^2 - \ell^2\right] + v_0\,, \qquad 0 < |x| \le \ell\,; \qquad \zeta \equiv -\frac{(\gamma-\alpha)}{\mathcal{D}_0\alpha^2}\,, \tag{2.14}$$

where v_0 is given in (2.11). This expression is a uniformly valid leading order solution for v on $|x| \le \ell$.

We summarize the results for our leading-order construction of a steady-state K-hotspot pattern as follows:

Proposition 2.1 *Let $\epsilon \to 0$, $q > 1$, and assume that $U_0 < S(\gamma-\alpha)$, as in (2.10). Then, (1.6) admits a steady-state solution on $(0, S)$ with K interior hotspots of a common amplitude. On each sub-domain of length $2\ell = S/K$, and translated to $(-\ell, \ell)$ to contain exactly one hotspot at $x = 0$, the steady-state solution, to leading order, is given by*

$$A \sim \frac{w(x/\epsilon)}{\epsilon\sqrt{v_0}}\,, \quad \text{if} \quad x = \mathcal{O}(\epsilon)\,; \qquad A \sim \alpha\,, \quad \text{if} \quad x = \mathcal{O}(1)\,, \tag{2.15a}$$

$$v \sim v_e = \frac{\zeta}{2}\left[(\ell - |x|)^2 - \ell^2\right] + v_0\,, \qquad \text{where} \quad v_0 = 2\pi^2 K^2\left[S(\gamma-\alpha) - U_0\right]^{-2}\,, \tag{2.15b}$$

$$u \sim \epsilon^{q-1}\tilde{u}_e\,, \qquad \text{where} \quad \tilde{u}_e \equiv \frac{U_0 v_0^{q/2}}{K I_q}\,, \qquad I_q \equiv \int_{-\infty}^{\infty} w^q\,dy = 2^{3q/2-1}\frac{[\Gamma(q/2)]^2}{\Gamma(q)}\,. \tag{2.15c}$$

Here $w(y) = \sqrt{2}\,\mathrm{sech}\,y$ is the homoclinic of (2.5).

In terms of the criminal and police densities, given respectively by $\rho = \epsilon^2 v A^2$ and $U = uA^q$ (see (1.3) and (1.5)), we can write (2.15) as follows:

Corollary 2.2 *Under the same conditions as in Proposition 2.1, (2.15) yields to leading-order that*

$$A \sim \frac{w(x/\epsilon)}{\epsilon\sqrt{v_0}}\,, \quad \text{if} \quad x = \mathcal{O}(\epsilon)\,; \qquad A \sim \alpha\,, \quad \text{if} \quad \mathcal{O}(\epsilon) \ll |x| < \ell\,, \tag{2.16a}$$

$$\rho \sim [w(x/\epsilon)]^2\,, \quad \text{if} \quad x = \mathcal{O}(\epsilon)\,; \qquad \rho \sim \epsilon^2 v_e \alpha^2\,, \quad \text{if} \quad \mathcal{O}(\epsilon) \ll |x| < \ell\,, \tag{2.16b}$$

$$U \sim \frac{U_0}{\epsilon K I_q}[w(x/\epsilon)]^q\,, \quad \text{if} \quad x = \mathcal{O}(\epsilon)\,; \qquad U \sim \epsilon^{q-1}\alpha^q\frac{U_0 v_0^{q/2}}{K I_q}\,, \quad \text{if} \quad \mathcal{O}(\epsilon) \ll |x| < \ell\,, \tag{2.16c}$$

where v_0 is given in (2.15) and $w(y) = \sqrt{2}\,\mathrm{sech}\,y$.

From (2.16), we observe that the criminal density near a hotspot is independent of the police deployment U_0 and patrol focus q. The maximum of the attractiveness is, however, decreased by increasing U_0.

To be done: Need a plot of the steady-state for A, ρ, and U.

3 Derivation of the NLEP for a K-Hotspot Steady-State Pattern

To analyze the linear stability of a K-hotspot steady-state solution, we must use asymptotic analysis to derive the corresponding nonlocal eigenvalue problem (NLEP). To do so, we first follow the methodology in [14] by deriving the NLEP for a one-hotspot solution on the reference domain $|x| \le \ell$, with Floquet-type boundary conditions imposed at $x = \pm\ell$. In terms of this reference problem, the NLEP for the finite-domain problem $0 < x < S$ with Neumann conditions at $x = 0, S$ is then readily recovered, as similar to that done in [14] for the basic crime model.

3.1 Linearization with Floquet Boundary Conditions

To study the linear stability of a K-hotspot steady-state we introduce the perturbation

$$A = A_e + e^{\lambda t}\phi\,, \qquad v = v_e + e^{\lambda t}\epsilon\psi\,, \qquad u = u_e + e^{\lambda t}\epsilon^q\eta\,, \tag{3.1}$$

where (A_e, v_e, u_e) is the steady-state with a single hotspot centered at the origin in $|x| \le \ell$. The orders of the perturbations ($\mathcal{O}(1)$, $\mathcal{O}(\epsilon)$ and $\mathcal{O}(\epsilon^q)$ for the A, v and u components, respectively) are chosen so that ϕ, ψ, and η are all $\mathcal{O}(1)$ in the inner region. Upon substituting (3.1) into (1.6) and linearizing, we obtain that

$$\epsilon^2\phi_{xx} - \phi + 3\epsilon^2 v_e A_e^2\phi + \epsilon^3 A_e^3\psi = \lambda\phi\,, \tag{3.2a}$$

$$\mathcal{D}_0\left(2A_e v_{ex}\phi + \epsilon A_e^2\psi_x\right)_x - 3\epsilon^2 A_e^2 v_e\phi - \epsilon^3 A_e^3\psi - q u_e A_e^{q-1}\phi - \epsilon^q\eta A_e^q = \lambda\epsilon^2\left(2A_e v_e\phi + \epsilon A_e^2\psi\right)\,, \tag{3.2b}$$

$$\mathcal{D}_0\left(qA_e^{q-1}\phi u_{ex} + \epsilon^q A_e^q\eta_x\right)_x = \epsilon^2\tau_u\lambda\left(qA_e^{q-1}u_e\phi + \epsilon^q A_e^q\eta\right)\,. \tag{3.2c}$$

For $K \ge 2$, we will impose for the long-range components in (3.2b) and (3.2c) the following Floquet-type boundary conditions at $x = \pm\ell$:

$$\begin{pmatrix} \eta(\ell) \\ \psi(\ell) \end{pmatrix} = z\begin{pmatrix} \eta(-\ell) \\ \psi(-\ell) \end{pmatrix}\,, \qquad \begin{pmatrix} \eta(\ell) \\ \psi(\ell) \end{pmatrix} = z\begin{pmatrix} \eta_x(-\ell) \\ \psi_x(-\ell) \end{pmatrix}\,, \tag{3.3}$$

where z is a complex-valued parameter. For the $K = 1$ case, considered separately in §3.3 below, we need only impose Neumann conditions at $x = \pm l$ for the perturbations. Here we treat the $K \ge 2$ case.

For $K \ge 2$, the NLEP associated with a K-hotspot pattern on $[-l, (2K-1)l]$ with *periodic boundary conditions*, on a domain of length $2Kl$, is obtained by setting $z^K = 1$, which yields

$$z_j = e^{2\pi i j/K}\,, \qquad j = 0, \ldots, K-1\,. \tag{3.4}$$

By using these values of z_j in (3.3) we would obtain the spectral problem for the linear stability of a K-hotspot solution on a domain of length $2Kl$ subject to periodic boundary conditions. The next step is then to relate the spectra of the periodic problem to the Neumann problem in such a way that the Neumann problem is still posed on a domain of length S (cf. [14]). As discussed in §3 of [14] for $K \ge 2$, this involves simply replacing $2K$ with K in (3.4). As such, our Floquet parameter in (3.3) for a hotspot steady-state on a domain of length $S = 2lK$, having $K \ge 2$ interior hotspots and Neumann boundary conditions at $x = 0$ and $x = S$ is $z = e^{\pi i j/K}$. With this value of z, we calculate the identity

$$\frac{(z-1)^2}{2z} = \mathrm{Re}(z) - 1 = \cos\left(\frac{\pi j}{K}\right) - 1\,, \quad j = 0, \ldots, K-1\,, \tag{3.5}$$

which is needed in our analysis below.

We now begin our derivation of the NLEP. For (3.2a), in the inner region where $A_e \sim \epsilon^{-1}w/\sqrt{v_0}$, $v_e \sim v_0$, and $\psi \sim \psi(0) \equiv \psi_0$, we obtain that

$$\Phi'' - \Phi + 3w^2\Phi + \frac{\psi(0)}{v_0^{3/2}}w^3 = \lambda\Phi\,. \tag{3.6}$$

Here $\Phi(y) = \phi(\epsilon y)$ is the leading order term for the inner expansion of ϕ. In contrast, in the outer region, we obtain to leading order from (3.2) that

$$\phi \sim \epsilon^3\alpha^3\psi/[\lambda + 1 - 3\epsilon^2\alpha^2 v_e] = \mathcal{O}(\epsilon^3), \qquad \psi_{xx} \approx 0\,, \qquad \eta_{xx} \approx 0\,. \tag{3.7}$$

To determine $\psi(0)$, which from (3.6) will yield the NLEP, we must first carefully derive appropriate jump conditions for ψ_x and η_x across the hotspot region centered at $x = 0$. This is done in the next sub-section.

3.2 Jump Conditions and the Derivation of the NLEP for $K \geq 2$

To derive the appropriate jump condition for ψ_x across the hotspot region, we integrate (3.2b) over an intermediate domain $-\delta < x < \delta$ with $\epsilon \ll \delta \ll 1$. We use the facts that $A_e \sim \epsilon^{-1} w/\sqrt{v_0}$, $\phi \sim \Phi(y)$, $A_e(\pm\delta) \sim \alpha$, and $u_e = \epsilon^{q-1}\tilde{u}_e$ as given in (2.15), to obtain, upon letting $\delta/\epsilon \to +\infty$, that

$$\begin{aligned}\epsilon \mathcal{D}_0 \alpha^2 \left[\psi_x\right]_0 + 2\mathcal{D}_0 \alpha \left[v_{ex}\phi\right]_0 &= 3\epsilon \int_{-\infty}^{\infty} w^2 \Phi \, dy + \frac{\epsilon\psi(0)}{v_0^{3/2}} \int_{-\infty}^{\infty} w^3 \, dy \\ &\quad + \frac{\epsilon q \tilde{u}_e}{v_0^{(q-1)/2}} \int_{-\infty}^{\infty} w^{q-1}\Phi \, dy + \frac{\epsilon\eta(0)}{v_0^{q/2}} \int_{-\infty}^{\infty} w^q \, dy + \mathcal{O}(\epsilon^2\lambda)\,,\end{aligned}$$

where we have introduced the notation $[a]_0 \equiv a(0^+) - a(0^-)$ to indicate that the evaluation is to be done with the outer solution. In addition, we have used the convenient shorthand notation that $\int (\dots) \equiv \int_{-\infty}^{\infty} (\dots)\, dy$. Since $\phi = \mathcal{O}(\epsilon^3)$ in the outer region from (3.7), we can neglect the second term on the left-hand side of the expression above. For eigenvalues for which $\lambda \ll \mathcal{O}(\epsilon^{-1})$, we obtain that

$$\mathcal{D}_0 \alpha^2 [\psi_x]_0 = 3\int w^2\Phi + \frac{\psi(0)}{v_0^{3/2}} \int w^3 + \frac{q\tilde{u}_e}{v_0^{(q-1)/2}} \int w^{q-1}\Phi + \frac{\eta(0)}{v_0^{q/2}} \int w^q \,. \tag{3.8}$$

Now from (3.2b), we use $\phi = \mathcal{O}(\epsilon^3)$ in the outer region, together the fact $\epsilon^q \eta A_e^q \ll \mathcal{O}(\epsilon)$ since $q > 1$. In this way, from (3.2b) and (3.8), we obtain the following leading-order BVP problem for ψ with a jump condition for ψ_x across $x = 0$:

$$\psi_{xx} = 0\,, \quad |x| \leq \ell\,; \qquad e_0 \left[\psi_x\right]_0 = e_1\psi(0) + e_2\eta(0) + e_3\,, \quad \psi(\ell) = z\psi(-\ell)\,, \quad \psi_x(\ell) = z\psi_x(-\ell)\,, \tag{3.9a}$$

where we have defined e_j, for $j = 0, \dots, 3$, by

$$e_0 \equiv \mathcal{D}_0\alpha^2\,, \qquad e_1 \equiv \frac{1}{v_0^{3/2}} \int w^3\,, \qquad e_2 \equiv \frac{1}{v_0^{q/2}} \int w^q\,, \qquad e_3 \equiv 3\int w^2\Phi + \frac{q\tilde{u}_e}{v_0^{(q-1)/2}} \int w^{q-1}\Phi\,. \tag{3.9b}$$

This BVP is defined in terms of $\eta(0)$, which itself must be calculated from a separate BVP. To formulate this additional BVP, we integrate (3.2c) over $-\delta < x < \delta$, with $\epsilon \ll \delta \ll 1$, and let $\delta/\epsilon \to \infty$ to obtain

$$\mathcal{D}_0 \epsilon^q \alpha^q \left[\eta_x\right]_0 + \mathcal{D}_0 q \alpha^{q-1} \mathcal{O}(\epsilon^{q+2}) = \epsilon^3 \tau_u \lambda \left[\frac{q\tilde{u}_\epsilon}{v_0^{(q-1)/2}} \int w^{q-1}\Phi + \frac{\eta(0)}{v_0^{q/2}} \int w^q\right]. \tag{3.10}$$

To achieve a distinguished balance in (3.10), we introduce $\hat{\tau}_u$ defined by

$$\hat{\tau}_u \equiv \epsilon^{q-3}\tau_u\,. \tag{3.11}$$

With this scaling, the police diffusivity $D_p \equiv \epsilon^{-2}\mathcal{D}_0/\tau_u$, is simply

$$D_p \equiv \epsilon^{q-5}\mathcal{D}_0/\hat{\tau}_u\,. \tag{3.12}$$

In this way, (3.10) yields the following jump condition for the outer solution:

$$\mathcal{D}_0 \alpha^q \left[\eta_x\right]_0 = \hat{\tau}_u \lambda \left[\frac{q\tilde{u}_e}{v_0^{(q-1)/2}} \int w^{q-1}\Phi + \frac{\eta(0)}{v_0^{q/2}} \int w^q\right]. \tag{3.13}$$

Now in the outer region we obtain from (3.2c) that

$$\mathcal{D}_0 \epsilon^q \alpha^q \eta_{xx} + \mathcal{O}(\epsilon^{q+2}) = \epsilon^2 \tau_u \lambda \left[\mathcal{O}(\epsilon^{q+2}) + \mathcal{O}(\epsilon^q)\right]. \tag{3.14}$$

We will consider the range of τ_u, and consequently $\hat{\tau}_u$, where

$$\tau_u \ll \mathcal{O}(\epsilon^{-2})\,, \qquad \text{for which} \qquad \hat{\tau}_u \ll \mathcal{O}(\epsilon^{q-5})\,. \tag{3.15}$$

For this range, (3.14) reduces to $\eta_{xx} \approx 0$ to leading order. In this way, we obtain using (3.13), the following BVP for the leading-order outer solution for η with a jump condition for η_x across $x = 0$:

$$\eta_{xx} = 0\,, \quad |x| \le \ell\,; \qquad d_0\,[\eta_x]_0 = d_1\eta(0) + d_2\,, \quad \eta(\ell) = z\eta(-\ell)\,, \quad \eta_x(\ell) = z\eta_x(-\ell)\,. \tag{3.16a}$$

Here the constants d_0, d_1, and d_2, are defined by

$$d_0 \equiv \mathcal{D}_0\alpha^q, \qquad d_1 \equiv \frac{\hat{\tau}_u\lambda}{v_0^{q/2}}\int w^q, \qquad d_2 \equiv \frac{\hat{\tau}_u\lambda q\tilde{u}_e}{v_0^{(q-1)/2}}\int w^{q-1}\Phi\,. \tag{3.16b}$$

To solve the BVPs (3.16) and (3.9), and in this way determine $\psi(0)$ and $\eta(0)$, we need to establish a simple lemma.

Lemma 3.1 *Consider the BVP for $y = y(x)$ on $-\ell < x < \ell$ given by*

$$y_{xx} = 0\,, \quad -\ell < x < \ell\,; \qquad f_0\,[y_x]_0 = f_1 y(0) + f_2\,; \qquad y(\ell) = zy(-\ell)\,, \quad y_x(\ell) = zy_x(-\ell)\,, \tag{3.17}$$

where f_0, f_1 and f_2, are nonzero constants, and let z satisfy (3.5). Then, $y(0)$ is given by

$$y(0) = f_2\left[\frac{f_0}{\ell}\frac{(z-1)^2}{2z} - f_1\right]^{-1} = -\frac{f_2}{f_0(1-\cos(\pi j/K))/\ell + f_1}\,. \tag{3.18}$$

Proof: Let $y_0 = y(0)$. The solution of this BVP is continuous but not differentiable at $x = 0$, and has the form

$$y(x) = \begin{cases} y_0 + A_+ x & \text{if } 0 < x < \ell\,, \\ y_0 + A_- x & \text{if } -\ell < x < 0\,, \end{cases}$$

where $y_0 \equiv y(0)$. Upon imposing the Floquet boundary conditions we obtain $A_+ = zA_-$ and $y_0 + A_+\ell = z\,(y_0 - A_-\ell) = zy_0 - A_+\ell$, which yields that $A_+ = (z-1)y_0/(2\ell)$. Then, upon imposing the jump condition across $x = 0$ we get

$$f_1y_0 + f_2 = f_0\,[y_x]_0 = f_0\,(A_+ - A_-) = \frac{f_0y_0}{2\ell}\,(z-1)\left(1 - \frac{1}{z}\right)\,.$$

Upon solving for $y(0)$, and recalling the identify (3.5), we obtain (3.18) for $y(0)$. ■

Upon using Lemma 3.1 with $f_0 = e_0$, $f_1 = e_1$, and $f_2 = e_2\eta(0) + e_3$, we calculate from (3.9) that

$$\psi(0) = -\frac{e_2\eta(0) + e_3}{e_0(1-\cos(\pi j/K))/\ell + e_1}\,. \tag{3.19}$$

Then, by applying Lemma 3.1 with $f_0 = d_0$, $f_1 = d_1$, and $f_2 = d_2$, we calculate from (3.16) that

$$\eta(0) = -\frac{d_2}{d_0(1-\cos(\pi j/K))/\ell + d_1}\,. \tag{3.20}$$

The final step in the derivation is to substitute (3.20) into (3.19) and simplify the resulting expression for $\psi(0)$ so as to express it explicitly in terms of the original parameters. This will identify the key coefficient $\psi(0)/v_0^{3/2}$ in (3.6).

We first define D_j by

$$D_j \equiv \frac{\mathcal{D}_0}{\ell}\left(1 - \cos\left(\frac{\pi j}{K}\right)\right)\,, \qquad j = 0, \ldots, K-1\,, \quad \text{where} \quad l = S/(2K)\,, \tag{3.21}$$

so that $D_j < D_{j+1}$ for any $0 = 1, 2, \ldots, K-2$. Then, by calculating e_0 and d_0 from (3.9b) and (3.16b), and substituting (3.20) into (3.19), we obtain

$$\psi(0) = -\frac{1}{D_j\alpha^2 + e_1}\left[e_3 - \frac{e_2 d_2}{D_j\alpha^q + d_1}\right]. \tag{3.22}$$

Then, by using the expression for $\tilde{u}_e$, as given in (2.8), we rewrite the expressions for e_1, e_2, e_3, d_1, and d_2 in (3.9b) and (3.16b), as

$$e_1 = \frac{\int w^3}{v_0^{3/2}}, \qquad e_2 = \frac{\int w^q}{v_0^{q/2}}, \qquad e_3 = 3\int w^2\Phi + \frac{U_0\sqrt{v_0}}{K}\frac{q\int w^{q-1}\Phi}{\int w^q}, \tag{3.23a}$$

$$d_1 = \hat{\tau}_u\lambda\frac{\int w^q}{v_0^{q/2}}, \qquad d_2 = \hat{\tau}_u\lambda\left(\frac{U_0\sqrt{v_0}}{K}\frac{q\int w^{q-1}\Phi}{\int w^q}\right). \tag{3.23b}$$

Upon substituting (3.23) into (3.22), we obtain after some algebra that

$$\mathcal{B}(\lambda) \equiv -\frac{\psi(0)}{v_0^{3/2}} = \frac{1}{\left(1 + v_0^{3/2}D_j\alpha^2/\int w^3\right)}\left[\frac{3\int w^2\Phi}{\int w^3} + \frac{v_0^{q/2}D_j\alpha^q}{v_0^{q/2}D_j\alpha^q + \hat{\tau}_u\lambda\int w^q}\left(\frac{U_0\sqrt{v_0}}{K\int w^3}\right)\left(\frac{q\int w^{q-1}\Phi}{\int w^q}\right)\right]. \tag{3.24}$$

We first consider the synchronous mode for which $j = 0$, and $\mathcal{D}_0 = 0$ from (3.21). In this case, upon substituting (3.24) into (3.6) we obtain the following NLEP for the synchronous mode $j = 0$:

$$L_0\Phi - 3w^3\frac{\int w^2\Phi}{\int w^3} = \lambda\Phi, \qquad \Phi \to 0 \quad \text{as} \quad |y| \to \infty. \tag{3.25}$$

From Lemma 3.2 of [14] it follows that any nonzero eigenvalue of (3.25) must satisfy $\mathrm{Re}(\lambda) < 0$. We summarize this result as follows:

Proposition 3.2 *For $\epsilon \to 0$, $K \geq 2$, $q > 1$, $\mathcal{D}_0 = \epsilon^2 D = \mathcal{O}(1)$, and $\tau_u \ll \mathcal{O}(\varepsilon^{-2})$, a K-hotspot steady-state solution for (1.6) is always linearly stable on an $\mathcal{O}(1)$ time-scale to synchronous perturbations of the hotspot amplitudes.*

Remark 3.3 *In the limit of a large diffusivity ratio, for the two-component Gierer-Meinhardt and Gray-Scott RD systems in 1-D, the dominant oscillatory temporal instability in the spike amplitudes is always due to the synchronous mode (cf. [34], [16]). In contrast, for our three-component RD system (1.6), Proposition 3.2 shows that synchronous mode is always linearly stable.*

Therefore, in our linear stability analysis we need only consider the asynchronous modes $j = 1, \ldots, K-1$, for which $D_j \neq 0$. For these modes, (3.24) motivates the introduction of new quantities $\chi_{0,j}$, $\chi_{1,j}$ and $\mathcal{C}_q(\lambda)$, defined by

$$\chi_{0,j} \equiv \frac{1}{1 + v_0^{3/2}D_j\alpha^2/\int w^3}, \qquad \chi_{1,j} \equiv \left(\frac{U_0\sqrt{v_0}}{K\int w^3}\right)\frac{\chi_{0,j}}{\mathcal{C}_q(\lambda)}, \qquad \mathcal{C}_q(\lambda) \equiv 1 + \frac{\hat{\tau}_u\lambda\int w^q}{v_0^{q/2}D_j\alpha^q}. \tag{3.26}$$

Then $\mathcal{B}(\lambda)$ in (3.24) can be written compactly as

$$\mathcal{B}(\lambda) \equiv -\frac{\psi(0)}{v_0^{3/2}} = \chi_{0,j}\frac{3\int w^2\Phi}{\int w^3} + \chi_{1,j}\frac{q\int w^{q-1}\Phi}{\int w^q}. \tag{3.27}$$

In this way, from (3.6) and (3.27), we obtain an NLEP with two nonlocal terms. The result is summarized as follows:

Proposition 3.4 *For $\epsilon \to 0$, $K \geq 2$, $q > 1$, $\mathcal{D}_0 = \epsilon^2 D = \mathcal{O}(1)$, and $\tau_u \ll \mathcal{O}(\varepsilon^{-2})$, the linear stability on an $\mathcal{O}(1)$ time-scale of a K-hotspot steady-state solution for (1.6), for the asynchronous modes $j = 1, \ldots, K-1$, is characterized by the spectrum of the following NLEP for $\Phi(y)$ with two nonlocal terms:*

$$L_0\Phi - \chi_{0,j}w^3\frac{3\int w^2\Phi}{\int w^3} - \chi_{1,j}w^3\frac{q\int w^{q-1}\Phi}{\int w^q} = \lambda\Phi, \qquad \textit{where} \qquad L_0\Phi \equiv \Phi'' - \Phi + 3w^2\Phi. \tag{3.28}$$

Here $\chi_{0,j}$ and $\chi_{1,j}$ are defined in (3.26), and $w(y) = \sqrt{2}\,\mathrm{sech}\, y$.

Next, we express $\chi_{0,j}$ and $\chi_{1,j}$ in the NLEP (3.28) in terms of the original parameters. To do so, we first substitute (2.11) for v_0 into the expression (3.26) for $\chi_{0,j}$ and $\chi_{1,j}$. This suggests that it is convenient to introduce two new quantities κ_q and ω defined by

$$\kappa_q \equiv \left(\int w^q\right)^{-1}\left(\frac{\sqrt{2}\pi\alpha K}{\omega}\right)^q, \qquad \text{where} \qquad \omega \equiv S(\gamma-\alpha)-U_0\,. \tag{3.29}$$

In terms of these new variables, (3.26) becomes

$$\chi_{0,j} = \left(1+\frac{\kappa_3 D_j}{\alpha}\right)^{-1}, \qquad \chi_{1,j} = \frac{U_0}{\omega \mathcal{C}_q(\lambda)}\chi_{0,j}\,, \qquad \mathcal{C}_q(\lambda) \equiv 1+\frac{\hat{\tau}_u\lambda}{D_j\kappa_q}\,. \tag{3.30}$$

Next, we proceed to reformulate (3.28) as an NLEP with a single nonlocal term. To do so, we use the special property of the local operator L_0 that $L_0 w^2 = 3w^2$ (cf. [14]). Owing to the decay of Φ and w as $|y|\to\infty$, and since L_0 is self-adjoint, we obtain from Green's identity that $\int\left(w^2 L_0\Phi - \Phi L_0 w^2\right)=0$. By using (3.28) for $L_0\Phi$, together with $L_0 w^2 = 3w^2$ and the integral ratio $\int w^5/\int w^3 = 3/2$ from (2.6), we conclude from this Greeen's identity that

$$\left(\frac{\int w^2\Phi}{\int w^3}\right)\left[\frac{9\chi_{0,j}}{2}+(\lambda-3)\right] = -\frac{3q\chi_{1,j}}{2}\left(\frac{\int w^{q-1}\Phi}{\int w^q}\right). \tag{3.31}$$

There are several interesting limiting cases of the key identity (3.31) for any eigenpair of the NLEP (3.28) with two nonlocal terms. Since $\chi_{1,j}$ is proportional to U_0 from (3.30), we first observe from (3.31) that for any eignpair for which $\int w^m\Phi \neq 0$ for any $m>0$, we must have $\lambda = 3-9\chi_{0,j}/2$ if and only if $U_0=0$. We remark that this recovers the result in equation (3.17) of [14] that the unique discrete eigenvalue of the linearization of a K-hotspot steady-state of the two-component "basic" crime model with no police is

$$\lambda = 3-\frac{9\chi_{0,j}}{2}\,, \tag{3.32}$$

where $\chi_{0,j}$ is defined in (3.30). By setting $\lambda=0$ in this expression, the stability threshold in equation (3.19) of [14] is recovered. This is discussed in more detail in §4.3 below.

A second special case of (3.31), which is examined in detail in §5, is when $q=3$, for which (3.31) becomes

$$\left(\frac{\int w^2\Phi}{\int w^3}\right)\left[\frac{9}{2}\left(\chi_{0,j}+\chi_{1,j}\right)+\lambda-3\right]=0\,. \tag{3.33}$$

Therefore, when $q=3$, and for any eigenpair Φ and λ of (3.28) with $\int w^2\Phi\neq 0$, we have that λ must satisfy

$$\frac{9}{2}\left(\chi_{0,j}+\chi_{1,j}\right)+\lambda-3=0\,. \tag{3.34}$$

By using (3.30) for $\chi_{1,j}$, we obtain after some algebra that (3.34) reduces to a quadratic equation for λ given by

$$c_2\lambda^2+c_1\lambda+c_0=0\,, \tag{3.35a}$$

where c_0, c_1, and c_2, are defined for $j=1,\ldots,K-1$ by

$$c_2 = \frac{\hat{\tau}_u}{3\chi_{0,j}D_j\kappa_3}\,, \qquad c_1 = \frac{\hat{\tau}_u}{D_j\kappa_3}\left(\frac{3}{2}-\frac{1}{\chi_{0,j}}\right)+\frac{1}{3\chi_{0,j}}\,, \qquad c_0 = \frac{3U_0}{2\omega}+\frac{3}{2}-\frac{1}{\chi_{0,j}}\,. \tag{3.35b}$$

In §5 we will analyze the implications of (3.35) for the possibility of Hopf bifurcations.

Since $U_0>0$, and since we only consider eignfunctions for which $\int w^m\Phi\neq 0$ for any $m>0$, we have $\lambda\neq 3-9\chi_{0,j}/2$. Therefore, in (3.31) we can isolate $\int w^2\Phi$ as

$$\frac{3\int w^2\Phi}{\int w^3} = \frac{-9}{9\chi_{0,j}+2(\lambda-3)}\left(\chi_{1,j}\frac{q\int w^{q-1}\Phi}{\int w^q}\right).$$

Upon substituting this expression back into (3.27) for $\beta(\lambda)$ we eliminate the nonlocal term $\int w^2\Phi$, and after some algebra conclude that

$$\beta(\lambda) = \chi(\lambda)\frac{\int w^{q-1}\Phi}{\int w^q}\,, \qquad \text{where} \qquad \chi(\lambda) \equiv q\chi_{1,j}\left(\frac{2(\lambda-3)}{9\chi_{0,j}+2(\lambda-3)}\right). \tag{3.36}$$

Finally, by substituting (3.30) for $\chi_{0,j}$ and $\chi_{1,j}$ into (3.36) we obtain our following main result for the NLEP with one nonlocal term:

Proposition 3.5 *For $\epsilon \to 0$, $K \geq 2$, $U_0 > 0$, $q > 1$, $\mathcal{D}_0 = \epsilon^2 D = \mathcal{O}(1)$, and $\tau_u \ll \mathcal{O}(\varepsilon^{-2})$, the linear stability on an $\mathcal{O}(1)$ time-scale of a K-hotspot steady-state solution for (1.6), for the asynchronous modes $j = 1, \ldots, K-1$, is is characterized by the spectrum of the NLEP for $\Phi(y)$ given by*

$$L_0\Phi - \chi(\lambda)w^3\frac{\int w^{q-1}\Phi}{\int w^q} = \lambda\Phi\,, \qquad \Phi \to 0 \quad as \quad |y| \to \infty\,, \tag{3.37a}$$

where $L_0\Phi \equiv \Phi'' - \Phi + 3w^2\Phi$. Here the multiplier $\chi(\lambda)$ of the NLEP is defined by

$$\chi(\lambda) \equiv \frac{qU_0}{\omega\mathcal{C}_q(\lambda)}\left(\frac{(\lambda-3)\chi_{0,j}}{(\lambda-3)+9\chi_{0,j}/2}\right), \qquad where \quad \frac{1}{\chi_{0,j}} = 1 + \frac{\kappa_3 D_j}{\alpha}\,, \quad and \quad \mathcal{C}_q(\lambda) = 1 + \frac{\hat{\tau}_u\lambda}{D_j\kappa_q}\,. \tag{3.37b}$$

Here κ_q and ω are defined in (3.29), D_j is defined in (3.21), and $\hat{\tau}_u$ is related to τ_u by (3.11).

Remark 3.6 *We observe that our NLEP (3.37) has the general form*

$$L_0\Phi - \left(\frac{a_0 + a_1\lambda}{b_0 + b_1\lambda + b_2\lambda^2}\right)w^3\frac{\int w^{q-1}\Phi}{\int w^q} = \lambda\Phi\,,$$

where the coefficients a_0, a_1, b_0, b_1 and b_2 are independent of λ. To our knowledge there have been no previous studies of NLEP's in 1-D where the multiplier χ of the NLEP is a proper rational function of degree two. Some results of this type are given in [28] for the linear stability analysis of spot patterns on the sphere for the Brusselator RD system.

The key model parameters we will use to analyze the NLEP are $\hat{\tau}_u$, q, U_0, $\mathcal{D}_0$, and ω. We remark that $\omega = U_{0,\max} - U_0$ where $U_{0,\max} = S(\gamma - \alpha)$ is the maximum police deployment for which a hotspot steady-state can exist.

3.3 Derivation of the NLEP for a Single Hotspot: $K = 1$ case

For $K \geq 2$, the NLEP (3.37) was derived by imposing Floquet boundary conditions at $x = \pm\ell$. For the case of a single hotspot, we can impose the Neumann boundary conditions directly at $x = \pm\ell$, as the Floquet analysis is not needed. With the same procedure as that leading to (3.9) and (3.16) above, we now obtain

$$\psi_{xx} = 0\,, \quad |x| \leq \ell\,; \qquad e_0\left[\psi_x\right]_0 = e_1\psi(0) + e_2\eta(0) + e_3\,, \qquad \psi_x(\pm\ell) = 0\,, \tag{3.38}$$

together with the BVP for $\eta(x)$, given by

$$\eta_{xx} = 0\,, \quad |x| \leq \ell\,; \qquad d_0\left[\eta_x\right]_0 = d_1\eta(0) + d_2\,, \qquad \eta_x(\pm\ell) = 0\,. \tag{3.39}$$

Here the coefficients e_0, e_1, e_2, e_3 and d_0, d_1 and d_2, are as defined in (3.9b) and (3.16b), respectively.

From these two problems it immediately follows that $\eta(x) = \eta(0)$ everywhere and that $\eta(0) = -d_2/d_1$. In addition, we find that $\psi(x) = \psi(0)$ everywhere, with $\psi(0)$ given by

$$\psi(0) = -\frac{1}{e_1}\left(e_2\eta(0) + e_3\right) = -\frac{1}{e_1}\left(e_3 - \frac{e_2 d_2}{d_1}\right).$$

This is precisely the formula given in (3.22) with D_j set to zero.

Therefore, by proceeding in the same way as done in the Floquet analysis performed earlier for the $K \geq 2$ case, we simply set D_j to zero in the expression (3.24), and in this way determine $\beta(\lambda)$ as

$$\beta \equiv -\frac{\psi(0)}{v_0^{3/2}} = \frac{3\int w^2\Phi}{\int w^3}\,. \tag{3.40}$$

By substituting (3.40) into (3.6) we obtain that the NLEP for a single hotspot solution is given by (3.25). For this NLEP, Lemma 3.2 of [14] proves that $\mathrm{Re}(\lambda) < 0$ for eigenfunctions for which $\int w^2\Phi \neq 0$. Therefore, we conclude that a single hotspot steady-state solution is unconditionally stable for any $\mathcal{D}_0$ when $\tau_u \ll \mathcal{O}(\epsilon^{-2})$.

3.4 Reformulation of the NLEP as Zeros of a Meromorphic Function

We now reformulate our NLEP (3.37) for a $K \geq 2$ hotspot steady-state so that its discrete eigenvalues are the zeros of a meromorphic function $\zeta(\lambda)$ in the right-half $\mathrm{Re}(\lambda) \geq 0$ of the complex plane. To do so, we first write (3.37) as

$$(L_0 - \lambda)\,\Phi = \chi(\lambda) w^3 \frac{\int w^{q-1}\Phi}{\int w^q}\,, \qquad \text{so that} \qquad \Phi = \chi(\lambda)\frac{\int w^{q-1}\Phi}{\int w^q}\,(L_0-\lambda)^{-1}\,w^3\,.$$

We then multiply both sides of this expression by w^{q-1} and integrate to get

$$\left(\int w^{q-1}\Phi\right)\left[1 - \chi(\lambda)\frac{\int w^{q-1}\,(L_0-\lambda)^{-1}\,w^3}{\int w^q}\right] = 0\,. \tag{3.41}$$

We conclude, provided that the eigenfunction satisfies $\int w^{q-1}\Phi \neq 0$, that an eigenvalue λ of the NLEP (3.37) must be a root of

$$\zeta(\lambda) \equiv \mathcal{C}(\lambda) - \mathcal{F}(\lambda) = 0\,, \qquad \text{where} \qquad \mathcal{F}(\lambda) \equiv \frac{\int w^{q-1}\,(L_0-\lambda)^{-1}\,w^3}{\int w^q}\,. \tag{3.42a}$$

Here $\mathcal{C}(\lambda) \equiv [\chi(\lambda)]^{-1}$, and from (3.37b) we have

$$\mathcal{C}(\lambda) = \frac{\omega\mathcal{C}_q(\lambda)}{qU_0}\left(\frac{1}{\chi_{0,j}} + \frac{9}{2(\lambda-3)}\right)\,, \tag{3.42b}$$

where $\chi_{0,j}$ and $\mathcal{C}_q(\lambda)$ are defined in (3.37b).

We will proceed to analyze the zeros of the meromorphic function $\zeta(\lambda) \equiv \mathcal{C}(\lambda) - \mathcal{F}(\lambda)$ in two cases: $q = 3$ and $q > 1$, with the former being explicitly solvable, and the latter requiring the Nyquist criterion to count the number of zeros in the unstable right half-plane $\mathrm{Re}(\lambda) > 0$. Moreover, we will also investigate the possibility of a Hopf bifurcation, by seeking a pure imaginary root of the form $\lambda_\pm = \pm i\lambda_I$ to (3.42) with $\lambda_I > 0$. Since $j = 1, \ldots, K-1$, such a Hopf bifurcation will correspond to an asynchronous temporal oscillation of the hotspot amplitudes.

Remark 3.7 *When $\int w^{q-1}\Phi = 0$, the NLEP (3.37) reduces to the local eigenvalue problem $L_0\Phi = \lambda\Phi$ with the extra condition $\int w^{q-1}\Phi = 0$. From Proposition 5.6 of [6], L_0 has exactly two discrete eigenvalues of L_0. One is $\Phi = w^2$ with $\lambda = 3$, arising from the identity $L_0 w^2 = 3w^2$, for which $\int w^{q-1}\Phi \neq 0$, while the other is the odd eigenfunction $\Phi = w'$ for which $\lambda = 0$ and $\int w^{q-1}\Phi = 0$. Therefore, since there are no instabilities associated with modes for which $\int w^{q-1}\Phi = 0$, the zeroes of $\zeta(\lambda)$, as defined in (3.42), in $Re(\lambda) > 0$ will determine any instability of the K-hotspot steady-state with $K \geq 2$.*

4 Analysis of the NLEP: Competition Instability

In order to analyze zero-eigenvalue crossings for the NLEP (3.37), as well as the possibility of Hopf bifurcations, in §4.1 we need to provide some global properties of $\mathcal{F}(\lambda)$, as defined in (3.42a), on both the non-negative real axis $\lambda \geq 0$ and on the non-negative imaginary axis $\lambda = i\lambda_I$ with $\lambda_I \geq 0$. In §4.2 we apply the winding number criterion of complex analysis to count the number of zeroes of $\zeta(\lambda)$, defined in (3.42), in the unstable right half-plane $\mathrm{Re}(\lambda) > 0$. With these properties, in §4.3 we study the competition stability threshold characterized by zero-eigenvalue crossings of the NLEP (3.37). Oscillatory instabilities for $q = 3$ and for general $q > 1$ due to a Hopf bifurcation are studied in detail in §5 and §6, respectively.

Before summarizing the global properties of $\mathcal{F}(\lambda)$, we first show that $\mathcal{F}(\lambda)$ can be found explicitly when $q = 3$ by using the identity $L_0 w^2 = 3w^2$. When $q = 3$, we calculate the integral I in the numerator for $\mathcal{F}(\lambda)$, given in (3.42a), as

$$I \equiv \int w^2 \left(L_0 - \lambda\right)^{-1} w^3 = \frac{1}{3} \int \left(L_0 w^2\right) \left(L_0 - \lambda\right)^{-1} w^3 = \int \left[(L_0 - \lambda) w^2 + \lambda w^2\right] \left(L_0 - \lambda\right)^{-1} w^3 \, .$$

Upon integrating this last expression by parts, we get the algebraic equation $I = \left(\int w^5 + \lambda I\right)/3$, so that $I = \int w^5/(3-\lambda)$. Then, since $\mathcal{F} = I/\int w^3$ and $\int w^5 / \int w^3 = 3/2$ from (2.6), we conclude that

$$\mathcal{F}(\lambda) = \frac{3}{2(3-\lambda)} \, , \qquad \text{when} \quad q = 3 \, . \tag{4.1}$$

4.1 Key Global and Asymptotic Properties of $\mathcal{F}(\lambda)$

We first recall some key properties of $\mathcal{F}(\lambda)$, defined in (3.42a), on the non-negative real axis $\lambda \geq 0$.

Proposition 4.1 *On the non-negative real axis $\lambda \geq 0$, $\mathcal{F}(\lambda)$ given in (3.42a) satisfies*

(i) $\mathcal{F}(\lambda) \sim \frac{1}{2} + \frac{\lambda}{4}\left(1 - \frac{1}{q}\right) + \mathcal{O}(\lambda^2) \quad$ *as* $\quad \lambda \to 0 \, .$

(ii) $\mathcal{F}(\lambda) \to +\infty \quad$ *as* $\quad \lambda \to 3^- \, .$

(iii) $\mathcal{F}'(\lambda) > 0 \, , \quad$ *for* $\quad 0 < \lambda < 3$, *when* $q = 2, 3, 4 \, .$

(iv) $\mathcal{F}(\lambda) < 0 \, , \quad$ *for* $\quad \lambda > 3 \, .$

Proof: The statements in (i), (ii), and (iv), as well as in (iii) for $q = 2$ and $q = 4$, were proved in Proposition 3.5 of [34]. For $q = 3$, the monotonicity result in (iii) is seen to hold by using the explicit form for $\mathcal{F}(\lambda)$ given in (4.1). ■

In addition to the results (i), (ii), and (iv), which hold for all $q > 1$, we conjecture that the monotonicity result in (iii) holds not just for $q = 2, 3, 4$ but for all integers $q > 1$. As additional support of this conjecture, in Fig. 1 we plot the numerically computed function $\mathcal{F}(\lambda)$ on $0 < \lambda < 3$ for $q = 2, 3, 4, 5$.

Conjecture 4.2 *The monotonocity property (iii) of Proposition 4.1 that $\mathcal{F}'(\lambda) > 0$ on $0 < \lambda < 3$ holds for all integers $q > 1$.*

Next, in order to count the number of eigenvalues of the NLEP (3.37) in $\mathrm{Re}(\lambda) > 0$ below, we need some properties of $\mathcal{F}(\lambda)$, as defined in (3.42a), as restricted to the non-negative imaginary axis. By rewriting the operator as

$$\left(L_0 - i\lambda_I\right)^{-1} = \left(L_0 + i\lambda_I\right) \left[\left(L_0 + i\lambda_I\right)^{-1} \left(L_0 - i\lambda_I\right)^{-1}\right] = L_0 \left[L_0^2 + \lambda_I^2\right]^{-1} + i\lambda_I \left[L_0^2 + \lambda_I^2\right]^{-1} \, ,$$

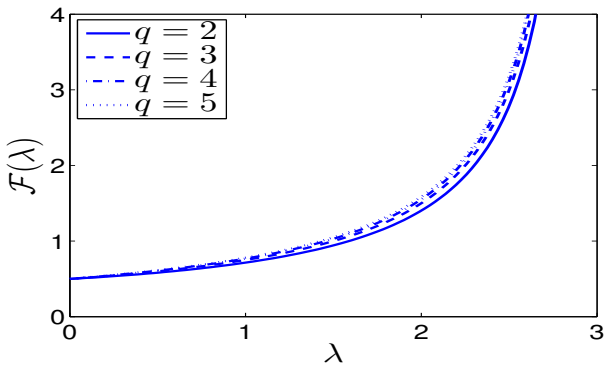

Figure 1: Plot of $\mathcal{F}(\lambda)$ on $0 < \lambda < 3$ for $q = 2, 3, 4, 5$. Note that $\mathcal{F}(0) = 1/2$ and that $\mathcal{F}(\lambda) \to +\infty$ as $\lambda \to 3$ from below. We observe that $\mathcal{F}(\lambda)$ is rather insensitive to changes in q.

we readily obtain upon upon separating $\mathcal{F}(i\lambda_I) = \int w^{q-1}(L_0 - i\lambda_I)^{-1} w^3 / \int w^q$ into real and imaginary parts that

$$\mathcal{F}(i\lambda_I) = \mathcal{F}_R(\lambda_I) + i\mathcal{F}_I(\lambda_I)\,; \qquad \mathcal{F}_R(\lambda_I) = \frac{\int w^{q-1} L_0 \left[L_0^2 + \lambda_I^2\right]^{-1} w^3}{\int w^q}\,, \qquad \mathcal{F}_I(\lambda_I) = \frac{\lambda_I \int w^{q-1} \left[L_0^2 + \lambda_I^2\right]^{-1} w^3}{\int w^q}\,. \tag{4.2}$$

We then recall some rigorous results of [34] for $\mathcal{F}_R(\lambda_I)$ and $\mathcal{F}_I(\lambda_I)$ on $\lambda_I \geq 0$.

Proposition 4.3 *For $\lambda = i\lambda_I$ with $\lambda_I > 0$, we have that $\mathcal{F}_R(\lambda_I)$ and $\mathcal{F}_I(\lambda_I)$ satisfy*

(i) $\mathcal{F}_R(\lambda_I) = \mathcal{O}(\lambda_I^{-2})$ *as* $\lambda_I \to +\infty\,, \quad \mathcal{F}_R(0) = 1/2.$

(ii) $\mathcal{F}_R'(\lambda_I) < 0\,,$ *when* $q = 2, 3\,.$

(iii) $\mathcal{F}_I(\lambda_I) = \mathcal{O}(\lambda_I^{-1})$ *as* $\lambda_I \to +\infty.$

(iv) $\mathcal{F}_I(\lambda_I) \sim \frac{\lambda_I}{4}\left(1 - \frac{1}{q}\right) > 0$ *as* $\lambda_I \to 0^+\,.$

(v) $\mathcal{F}_I(\lambda_I) > 0\,,$ *when* $q = 2, 3, 4.$

Proof: The statement in (i), and in (ii) for $q = 2$, were proved in Proposition 3.1 of [34]; (iii), (iv), and (v) for $q = 2, 4$, were proved in Proposition 3.2 of [34]. The results in (ii) and (v) for $q = 3$ follow by using the explicit formula in (4.1). For $q = 3$, we have $\mathcal{F}(i\lambda_I) = 3/\left[2(3 - i\lambda_I)\right]$, so that

$$\mathcal{F}_R(\lambda_I) = \frac{9}{2(9 + \lambda_I^2)}\,, \quad \mathcal{F}_R'(\lambda_I) = -\frac{9\lambda_I}{(9 + \lambda_I^2)^2}\,, \quad \mathcal{F}_I(\lambda_I) = \frac{3\lambda_I}{2(9 + \lambda_I^2)}\,, \quad \mathcal{F}_I'(\lambda_I) = \frac{3(9 - \lambda_I^2)}{2(9 + \lambda_I^2)^2}\,, \quad \text{for} \quad q = 3\,. \tag{4.3}$$

This clearly shows that properties (ii) and (v) also hold for $q = 3$. Moreover, it follows that $\mathcal{F}_I$ has a unique local maximum at the principal eigenvalue $\lambda_I = 3$ of L_0. ■

Although we only have a rigorous proof that $\mathcal{F}_R'(\lambda_I) < 0$ when $q = 2, 3$ and that $\mathcal{F}_I(\lambda_I) > 0$ when $q = 2, 3, 4$, we now conjecture that these key properties hold for all integers $q > 1$. In Fig. 2 we plot the numerically computed functions $\mathcal{F}_R(\lambda_I)$ and $\mathcal{F}_I(\lambda_I)$ for various values of q, which give numerical evidence for this conjecture. From this figure we observe that $\mathcal{F}_R(\lambda_I)$ is rather insensitive to changes in q.

Conjecture 4.4 *The properties (ii) and (v) in Proposition 4.3 that $\mathcal{F}_R'(\lambda_I) < 0$ and $\mathcal{F}_I(\lambda_I) > 0$ on $\lambda_I > 0$ hold for all* integers $q > 1$.

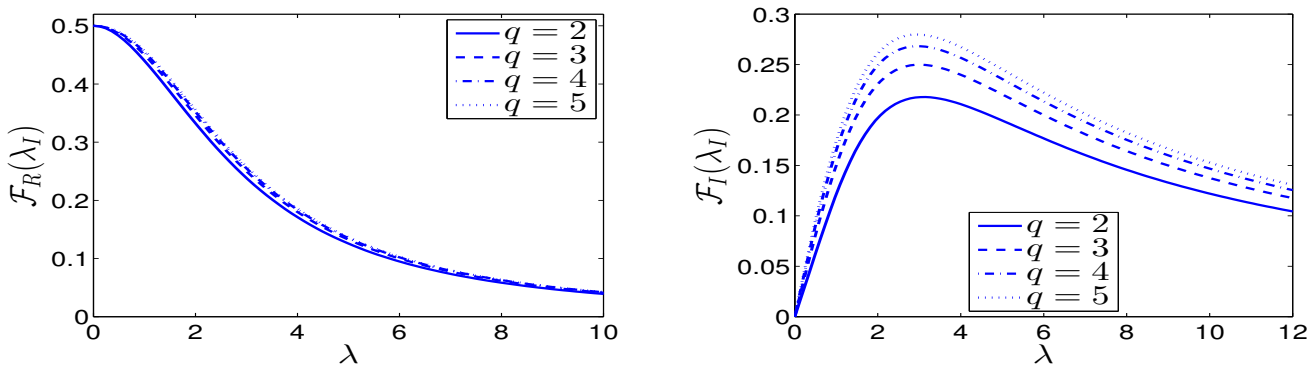

Figure 2: Plots of $\mathcal{F}_R(\lambda_I)$ (left panel) and $\mathcal{F}_I(\lambda_I)$ (right panel) for $q = 2, 3, 4, 5$. Note that $\mathcal{F}_R(0) = 1/2$ and $\mathcal{F}_I(0) = 0$, and that the maximum of $\mathcal{F}_I$ occurs near $\lambda_I = 3$. In fact, the maximum does occur exactly at $\lambda_I = 3$ when $q = 3$.

4.2 A Winding Number Criterion for the Number of Unstable Eigenvalues of the NLEP

We now use the argument principle of complex analysis to count the number N of eigenvalues of the NLEP (3.37) in $\mathrm{Re}(\lambda) > 0$. For each $j = 1, \ldots, K-1$, these discrete eigenvalues are the complex zeroes of the function $\zeta(\lambda) \equiv \mathcal{C}(\lambda) - \mathcal{F}(\lambda)$, as defined in (3.42). Here $\mathcal{F}(\lambda)$ is defined in (3.42a) and from (3.42b) we have that $\mathcal{C}(\lambda)$ has the explicit form

$$\mathcal{C}(\lambda) = a(1 + \tilde{\tau}_{u,j}\lambda)\left(1 - \frac{b}{3-\lambda}\right), \tag{4.4a}$$

where a, b, and $\tilde{\tau}_{u,j}$, are defined for $j = 1, \ldots, K-1$ by

$$a \equiv \frac{\omega}{qU_0\chi_{0,j}}, \qquad b \equiv \frac{9}{2}\chi_{0,j}, \qquad \tilde{\tau}_{u,j} \equiv \frac{\hat{\tau}_u}{D_j\kappa_q}, \qquad \frac{1}{\chi_{0,j}} = 1 + \frac{\kappa_3 D_j}{\alpha}. \tag{4.4b}$$

Here ω and κ_q are given in (3.29), while D_j and $\hat{\tau}_u$ are defined in (3.21) and 3.11, respectively.

We observe from (4.4a) that $\mathcal{C}(\lambda)$ is a meromorphic function with a simple pole at $\lambda = 3$. Moreover, $\mathcal{F}(\lambda)$ is analytic in $\mathrm{Re}(\lambda) \geq 0$ except at the simple pole at $\lambda = 3$. The simple poles of $\mathcal{C}(\lambda)$ and $\mathcal{F}(\lambda)$ do not cancel as $\lambda \to 3^-$, since when restricted to the real line we get $\mathcal{F}(\lambda) \to +\infty$ while $\mathcal{C}(\lambda) \to -\infty$ as $\lambda \to 3^-$. Thus, $\zeta(\lambda) = \mathcal{C}(\lambda) - \mathcal{F}(\lambda)$ has a simple pole at $\lambda = 3$.

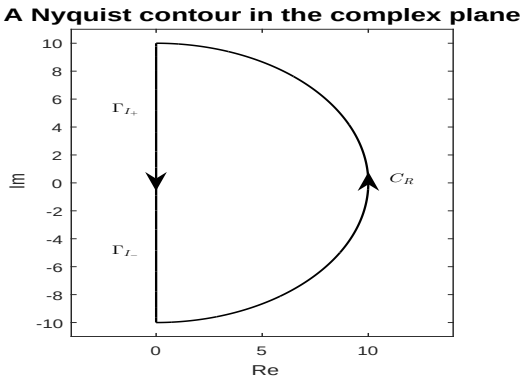

Figure 3: Schematic plot of the Nyquist contour Γ used for determining the number N of unstable eigenvalues of the NLEP (3.37).

To determine a formula for N, we calculate the winding of $\zeta(\lambda)$ over the Nyquist contour Γ traversed in the counterclockwise direction that consists of the following segments in the complex λ-plane (see the schematic in Fig. 3): Γ_I^+ ($0 < \mathrm{Im}(\lambda) < iR$, $\mathrm{Re}(\lambda) = 0$), Γ_I^- ($-iR < \mathrm{Im}(\lambda) < 0$, $\mathrm{Re}(\lambda) = 0$), and C_R defined by $|\lambda| = R > 0$ for $|\arg(\lambda)| < \pi/2$.

For each $j = 1, \ldots, K-1$, $\zeta(\lambda)$ is analytic in $\mathrm{Re}(\lambda) \geq 0$ except at the simple pole $\lambda = 3$ corresponding to the unique positive eigenvalue of the local operator L_0. Therefore, for each $j = 1, \ldots, N-1$, and assuming that $\zeta(\lambda)$ has no zeroes on the imaginary axis, we have by the argument principle that $N = 1 + (2\pi)^{-1} \lim_{R\to\infty} [\arg\zeta]_\Gamma$, where $[\arg\zeta]_\Gamma$ denotes the change in the argument of ζ over Γ. Since $\mathcal{F}(\lambda) = \mathcal{O}(|\lambda|^{-1})$ on the semi-circle C_R as $R = |\lambda| \to \infty$, we have that $\lim_{R\to\infty} [\arg\zeta]_{C_R} = \lim_{R\to\infty} [\arg\mathcal{C}]_{C_R}$. From (4.4a) we calculate that $\lim_{R\to\infty} [\arg\mathcal{C}]_{C_R} = \pi$ when $\hat{\tau}_u > 0$, and $\lim_{R\to\infty} [\arg\mathcal{C}]_{C_R} = 0$ when $\hat{\tau}_u = 0$. For the contour Γ_I^-, we use that $\zeta(\overline{\lambda}) = \overline{\zeta(\lambda)}$ so that $[\arg\zeta]_{\Gamma_I^-} = [\arg\zeta]_{\Gamma_I^+}$. In this way, for each $j = 1, \ldots, K-1$, we conclude that

$$N = \frac{3}{2} + \frac{1}{\pi}[\arg\zeta]_{\Gamma_I^+}\,, \quad \text{for} \quad \hat{\tau}_u > 0\,; \qquad N = 1 + \frac{1}{\pi}[\arg\zeta]_{\Gamma_I^+}\,, \quad \text{for} \quad \hat{\tau}_u = 0\,. \tag{4.5}$$

Here $[\arg\zeta]_{\Gamma_I^+}$ denotes the change in the argument of g_j as the imaginary axis $\lambda = i\lambda_I$ is traversed from $\lambda_I = +\infty$ to $\lambda_I = 0$.

We remark that (4.5) determines the number of unstable eigenvalues of the NLEP (3.37) for any *specific* asynchronous mode $j = 1, \ldots, K-1$. The total number of such unstable eigenvalues, for all asynchronous modes, is simply the union of (4.5) over $j = 1, \ldots, K-1$. In this way, the problem of determining N for a particular mode j is reduced to calculating the change of argument of $\zeta(\lambda) = \mathcal{C}(\lambda) - \mathcal{F}(\lambda)$ as we traverse down the positive imaginary axis. To do so, we will need the properties of $\mathcal{F}(i\lambda_I)$ given in Proposition 4.3, together with results for $\mathcal{C}(i\lambda)$ to be obtained from (4.4).

4.3 The Competition Instability Threshold

We now determine the competition instability threshold value of the diffusivity $\mathcal{D}_0$, which is characterized by a zero eigenvalue crossing of the NLEP (3.37). Since $\mathcal{F}(0) = 1/2$ (see (i) and (iv) of Proposition 4.3), we conclude that $\zeta(0) = 0$ when $\mathcal{C}(0) = 1/2$. From using (3.42b), or equivalently (4.4), for $\mathcal{C}(\lambda)$ we conclude that $\lambda = 0$ when

$$\frac{\omega}{qU_0}\left(\frac{1}{\chi_{0,j}} - \frac{3}{2}\right) = \frac{1}{2}\,, \qquad j = 1, \ldots, K-1\,. \tag{4.6}$$

By using (4.4b) for $\chi_{0,j}$, together with (3.29) for κ_3, (4.6) yields that $\lambda = 0$ when

$$D_j = \frac{\omega^3}{4\pi^2 K^3 \alpha^2}\left(1 + \frac{qU_0}{\omega}\right)\,, \qquad j = 1, \ldots, K-1\,. \tag{4.7}$$

Finally, by using $D_j = 2K\mathcal{D}_0(1 - \cos(\pi j/K))/S$, as obtained from (3.21), we conclude that the NLEP has a zero eigenvalue crossing at the $K-1$ distinct values $\mathcal{D}_{0,j}$ of $\mathcal{D}_0$ given by

$$\mathcal{D}_{0,j} = \frac{\omega^3 S}{8\pi^2\alpha^2 K^4\left(1 - \cos\left(\pi j/K\right)\right)}\left(1 + \frac{qU_0}{\omega}\right)\,, \qquad j = 1, \ldots, K-1\,. \tag{4.8}$$

As we show in Proposition 4.6 below, the competition instability threshold $\mathcal{D}_{0,c}$ corresponds to the smallest such $\mathcal{D}_{0,j}$, which occurs when $j = K-1$. This yields that

$$\mathcal{D}_{0,c} \equiv \mathcal{D}_{0,K-1} = \frac{\omega^3 S}{8\pi^2\alpha^2 K^4\left(1 + \cos\left(\pi/K\right)\right)}\left(1 + \frac{qU_0}{\omega}\right)\,. \tag{4.9}$$

In terms of the unscaled diffusivity $D = \epsilon^{-2}\mathcal{D}_0$, the competition stability threshold occurs at $D_c \equiv \epsilon^{-2}\mathcal{D}_{0,c}$.

Remark 4.5 *The zero-eigenvalue crossing condition (4.6) can also be obtained from the NLEP (3.28) with two nonlocal terms by setting $\Phi = w$ and $\lambda = 0$ in (3.28). By using the identity $L_0 w = 2w^3$, this substitution yields $2 - 3\chi_{0,j} - q\chi_{1,j} = 0$, where from (3.30) we have $\chi_{1,j} = U_0\chi_{0,j}/\omega$ at $\lambda = 0$. Some simple algebra then recovers (4.6).*

We now state our main instability result related to zero-eigenvalue crossings:

Proposition 4.6 *For $\epsilon \to 0$, $K \geq 2$, $U_0 > 0$, $q > 1$, $\mathcal{D}_0 = \epsilon^2 D = \mathcal{O}(1)$, a K-hotspot steady-state solution for (1.6) is unstable for all $\hat{\tau}_u \geq 0$ when $\mathcal{D}_0 > \mathcal{D}_{0,c}$, where $\mathcal{D}_{0,c}$ is the competition stability threshold defined in (4.9). For $\mathcal{D}_0 < \mathcal{D}_{0,c}$, a K-hotspot steady-state is linearly stable when $\hat{\tau}_u = 0$ and $q = 2, 3, 4$.*

Proof: We first prove that when $\mathcal{D}_0 > \mathcal{D}_{0,c}$, then $\zeta(\lambda) = 0$ in (3.42) has a positive real root in $0 < \lambda < 3$ for each $j = 1, \ldots, K-1$. This readily follows from the fact that $\mathcal{C}(0) > 1/2$ for each $j = 1, \ldots, K-1$, and from Proposition 4.1 where we have $\mathcal{F}(0) = 1/2$ and $\mathcal{F}(\lambda) \to +\infty$ as $\lambda \to 3^-$. Thus, by continuity, there is at least one positive real root to $\zeta(\lambda) = 0$ on $0 < \lambda < 3$ for each $j = 1, \ldots, K-1$ and for any $\hat{\tau}_u \geq 0$. Next, for $\mathcal{D}_0 < \mathcal{D}_{0,c}$, we show that $N = 0$ by using the winding number criterion (4.5) and calculating $[\arg \zeta]_{\Gamma_I^+}$ explicitly. From (4.4a), we decompose $\mathcal{C}(i\lambda_I) = \mathcal{C}_R(\lambda_I) + i\mathcal{C}_I(\lambda_I)$, and for $\hat{\tau}_u = 0$ calculate that

$$\mathcal{C}_I(\lambda_I) = -\frac{ab\lambda_I}{9 + \lambda_I^2} < 0 \qquad \text{for} \quad \lambda_I > 0\,.$$

Since $\mathcal{F}_I(\lambda_I) > 0$ for $\lambda_I > 0$ for $q = 2, 3, 4$ from property (v) of Proposition 4.3, we conclude that $\mathrm{Im}\zeta(i\lambda_I) < 0$ for $\lambda_I > 0$. Then, since $\mathcal{C}(0) > 1/2$ when $\mathcal{D}_0 < \mathcal{D}_{0,c}$, and $\mathcal{F}(0) = 1/2$ from (i) of Proposition 4.1, we have $\zeta(0) > 0$ for each $j = 1, \ldots, K-1$, and $\zeta(i\lambda_I) \to \omega/(qU_0\chi_{0,j}) > 0$ as $\lambda_I \to +\infty$. It follows that $[\arg \zeta]_{\Gamma_I^+} = -\pi$, and consequently $N = 0$ from the second statement in (4.5) for $\hat{\tau}_u = 0$. ■

We remark that if Conjecture 4.4 holds, then a K-hotspot steady-state is linearly stable when $\mathcal{D}_0 < \mathcal{D}_{0,c}$ and $\hat{\tau}_u = 0$ for any $q > 1$. Moreover, by continuity of eigenvalue paths in $\hat{\tau}_u$, the stability result in Proposition 4.6 should hold for all $\hat{\tau}_u > 0$ but sufficiently small. The possibility of Hopf bifurcations values of $\hat{\tau}_u$ for the range $\mathcal{D}_0 < \mathcal{D}_{0,c}$ is examined for $q = 3$ in §5 and for general $q > 1$ in §6.

4.4 Qualitative Interpretation of the Competition Instability Threshold

Next, we discuss the qualitative behavior of the competition instability threshold $\mathcal{D}_{0,c}$ with respect to the degree q of patrol focus, and the total level U_0 of police patrol deployment.

We recall from (2.12) that the maximum $A_{\max}$ of the steady-state attractiveness field is $A_{\max} \sim \epsilon^{-1}\omega/(K\pi)$, which decreases as either ω decreases or K increases. However, from Corollary 2.2, the amplitude of the steady-state criminal density ρ at the hotspot locations is $\rho_{\max} = [w(0)]^2 = 2$, which is independent of all model parameters, while away from the maxima of A the criminal density is $\mathcal{O}(\epsilon^2) \ll 1$. Therefore, it is the reduction of the number of stable steady-state hotspots on a given domain length that is the primary factor in reducing the total crime in the domain. As such, we seek to tune the police parameters q and U_0 so that the range of diffusivity $\mathcal{D}_0$ for which a K-hotspot steady-state is unconditionally unstable, i.e. unstable for all $\hat{\tau}_u > 0$, is as large as possible. This corresponds to minimizing the competition stability threshold $\mathcal{D}_{0,c}$ in (4.9).

From (4.9), we observe that $\mathcal{D}_{0,c}$ increases with q in a linear fashion. Within the context of our RD model (1.6), this predicts that if the police become increasingly focused on patrolling the more crime-attractive areas, then paradoxically the range of $\mathcal{D}_0$ where a K-hotspot steady-state is unstable decreases. Therefore, for the goal of reducing the number of stable crime hotspots, a police deployment with intense focus on crime-attractive areas does not offer an advantage over that of a less focused patrol (assuming that $q > 1$ for our analysis to hold). At a fixed level U_0 of police deployment, and for integers $q > 1$, the best patrol strategy is to take $q = 2$, which corresponds to the "cops-on-the-dots" strategy (cf. [12], [26], [38]) where the police mimic the movement of the criminals.

For a fixed $q > 1$, we next examine how the competition stability threshold for a K-hotspot steady-state changes with

the total police deployment U_0. To this end, we substitute $U_0 = S(\gamma - \alpha) - \omega$ into (4.9), and write $\mathcal{D}_{0,c}$ as

$$\mathcal{D}_{0,c} = \frac{S}{8\pi^2\alpha^2 K^4\,(1+\cos(\pi/K))}\,g(U_0)\,, \qquad g(U_0) \equiv \omega^3(1-q) + qS(\gamma-\alpha)\omega^2\,; \qquad \omega \equiv S(\gamma-\alpha) - U_0\,. \tag{4.10}$$

To analyze the critical points of $g(U_0)$, we first observe that $d\omega/dU_0 = -1$ and that $U_0 \to U_{0,\max} = S(\gamma-\alpha)$ as $\omega \to 0$. We then calculate that

$$\frac{dg}{dU_0} = -3(1-q)\omega\,(\omega - \omega_c)\,, \qquad \text{where} \qquad \omega_c \equiv \frac{2qS(\gamma-\alpha)}{3(q-1)}\,.$$

We conclude that $\omega_c < S(\gamma-\alpha)$, so that $0 < U_0 < U_{0,\max}$, iff $q > 3$. Therefore, $g(U_0)$ has a unique maximum point on $0 < U_0 < U_{0,\max}$ iff $q > 3$. Alternatively, for $q \le 3$ we have $dg/dU_0 < 0$ for $0 < U_0 < U_{0,\max}$.

This shows that if the degree of patrol focus q satisfies $q \le 3$, then $\mathcal{D}_{0,c}$ is monotonically decreasing in U_0. Therefore, for this range of q, increasing the level U_0 of police deployment leads to a larger range of $\mathcal{D}_0$ where the K-hotspot steady-state is unconditionally unstable. However, if $q > 3$, then initially as the level of police deployment is increased from zero, the range of $\mathcal{D}_0$ where the steady-state hotspot pattern is unstable is decreased, until the critical value

$$U_{0,c} \equiv S(\gamma-\alpha) - \omega_c = S(\gamma-\alpha)\frac{(q-3)}{3(q-1)}\,, \qquad q > 3\,, \tag{4.11}$$

is reached. For $U_0 > U_{0,c}$, the hotspot pattern becomes less stable when the policing level is increased. These qualitative results are displayed graphically in Fig. 4.

Finally, we can interpret our competition stability threshold in terms of a critical threshold K_c for which a steady-state pattern of $K \ge 2$ hotspots is unconditionally unstable when $K > K_c$. This instability, which develops on an $\mathcal{O}(1)$ time scale as $\varepsilon \to 0$, is due to a real positive eigenvalue of the NLEP, and as we show from full numerical simulations in §4.5 it triggers the collapse of some of the hotspots in the pattern. By writing (4.10) in terms of K, this critical threshold $K_c > 0$ when $D = \mathcal{D}_0/\epsilon^2$, and where $g(U_0)$ is defined in (4.10), is the unique root of

$$K\,[1+\cos(\pi/K)]^{1/4} = \frac{(S/D)^{1/4}}{2^{3/4}\sqrt{\pi\epsilon\alpha}}\,[g(U_0)]^{1/4}\,. \tag{4.12}$$

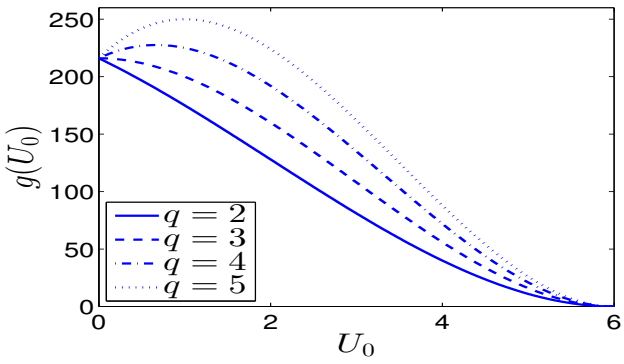

Figure 4: Competition instability threshold nonlinearity $g(U_0)$, as defined in (4.10), versus total police deployment U_0 for patrol focus parameters $q = 2, 3, 4, 5$. Other model parameters are $S = 6$, $\gamma = 2$, $\alpha = 1$, so that $U_{0,\max} = 6$ as shown in the right-most tick of the figure. The competition instability threshold $\mathcal{D}_{0,c}$ is simply a positive scaling of $g(U_0)$ according to (4.10).

4.5 Numerical Validation: Competition Instability

To be written once I get the full numerics for the PDE system working.

5 Explicitly Solvable Case $q = 3$: Asynchronous Hotspot Oscillations

For each $j = 1, \ldots, K-1$, we now analyze the quadratic equation (3.35) in the eigenvalue parameter λ characterizing the discrete spectrum of the NLEP (3.37) for the special case where $q = 3$. In terms of the coefficients of the quadratic (3.35a), for each $j = 1, \ldots, K$ the eigenvalues λ_1 and λ_2 satisfy

$$\lambda_1 \lambda_2 = \frac{c_0}{c_2}\,, \qquad \lambda_1 + \lambda_2 = -\frac{c_1}{c_2}\,, \tag{5.1}$$

where c_0, c_1, $c_2 > 0$ are given in (3.35b). For the j-th mode, we conclude that $\mathrm{Re}(\lambda) < 0$ when $c_0 > 0$ and $c_1 > 0$. We have instability of the j-th mode if either $c_0 < 0$, or if $c_0 > 0$ and $c_1 < 0$. We have purely complex eigenvalues, corresponding to a Hopf bifurcation point, when $c_0 > 0$ and $c_1 = 0$.

We first determine the signs of c_0 and c_1 in terms of D_j and $\hat{\tau}_u$. From (3.35b) we observe that $c_0 = 0$ when the zero-eigenvalue crossing condition (4.6) holds, which yields (4.7) for D_j, which we relabel as

$$D_j = D^{\star}_{\mathrm{up}} \equiv \frac{\omega^3}{4\pi^2 K^3 \alpha^2}\left(1 + \frac{3U_0}{\omega}\right). \tag{5.2}$$

Next, we set $c_1 = 0$ in (3.35b) to get, using (3.30) for $\chi^{-1}_{0,j}$, that

$$\frac{\hat{\tau}_u}{D_j \kappa_3} = \frac{2\chi^{-1}_{0,j}}{3\left(2\chi^{-1}_{0,j} - 3\right)} = \frac{1}{3}\frac{(D_j + \alpha/\kappa_3)}{(D_j - \alpha/(2\kappa_3))}\,. \tag{5.3}$$

The denominator of this expression motivates introducing $D^{\star}_{\mathrm{low}}$, defined by

$$D^{\star}_{\mathrm{low}} \equiv \frac{\alpha}{2\kappa_3} = \frac{\omega^3}{4\pi^2 K^3 \alpha_2}\,, \tag{5.4}$$

where we have used the expression (3.29) for κ_3. Upon using (5.4) in (5.3), we obtain that $c_1 = 0$ when $\hat{\tau}_u$ satisfies

$$\hat{\tau}_u = \hat{\tau}_{uH,j} \equiv \mathcal{H}\left(D_j/D^{\star}_{\mathrm{low}}\right), \qquad j = 1, \ldots, K-1\,, \tag{5.5a}$$

where the function $\mathcal{H}(\beta)$ is defined by

$$\mathcal{H}(\beta) \equiv \frac{\alpha\beta}{2}\left(\frac{1}{3} + \frac{1}{\beta - 1}\right). \tag{5.5b}$$

Notice that $\hat{\tau}_{uH,j} > 0$ only when $D_j > D^{\star}_{\mathrm{low}}$. Some simple algebra then shows that we can write c_1 in (3.35b) as

$$c_1 = \frac{1}{\alpha}\left(\frac{D^{\star}_{\mathrm{low}}}{D_j} - 1\right)\left(\hat{\tau}_u - \hat{\tau}_{uH,j}\right). \tag{5.6}$$

For the j-th mode, we have $c_1 < 0$ if $D_j > D^{\star}_{\mathrm{low}}$ and $\hat{\tau}_u > \hat{\tau}_{uH,j}$, while $c_1 > 0$ if either $D_j < D^{\star}_{\mathrm{low}}$, or $D_j > D^{\star}_{\mathrm{low}}$ and $\hat{\tau}_u < \hat{\tau}_{uH,j}$. With these signs for c_0 and c_1, we summarize our stability result for the j-th mode so far as follows:

- For $D_j > D^{\star}_{\mathrm{up}}$ ($c_0 < 0$), we have $\mathrm{Re}(\lambda) > 0$, and instability is due to a positive real eigenvalue.
- For $D_j < D^{\star}_{\mathrm{low}}$ ($c_0 > 0$ and $c_1 < 0$), we have stability $\mathrm{Re}(\lambda) < 0$.
- On the range $D^{\star}_{\mathrm{low}} < D_j < D^{\star}_{\mathrm{up}}$ ($c_0 > 0$), we have instability if $\hat{\tau}_u > \hat{\tau}_{uH,j}$ ($c_1 < 0$) and stability if $\hat{\tau}_u < \hat{\tau}_{uH,j}$ ($c_1 > 0$). On this range of D_j, the Hopf bifurcation threshold $\hat{\tau}_{uH,j} > 0$, is given in (5.5).

Next, we must reformulate this result in terms of $\mathcal{D}_0$ rather than D_j, by using $D_j = \mathcal{D}_0\,(2K/S)\,(1 - \cos(\pi j/K))$. The interval $D^{\star}_{\mathrm{low}} < D_1 < D^{\star}_{\mathrm{up}}$, where a Hopf bifurcation value of $\hat{\tau}_u$ exists, becomes

$$\frac{SD^{\star}_{\mathrm{low}}}{2K\left(1 - \cos(\pi j/K)\right)} \le \mathcal{D}_0 \le \frac{SD^{\star}_{\mathrm{up}}}{2K\left(1 - \cos(\pi j/K)\right)}\,, \tag{5.7}$$

where $D^\star_{\rm up}/D^\star_{\rm low} = 1 + 3U_0/\omega$ from (5.2) and (5.4). It is convenient to write (5.7) in terms of the competition stability threshold $\mathcal{D}_{0,c}$ defined by setting $q = 3$ in (4.9). In this way, the interval in (5.7) becomes

$$D^-_{0,j} < \mathcal{D}_0 < D^+_{0,j}\,; \qquad D^+_{0,j} \equiv \mathcal{D}_{0,c}\left(\frac{1+\cos(\pi/K)}{1-\cos(\pi j/K)}\right), \qquad D^-_{0,j} \equiv \frac{\mathcal{D}_{0,c}}{(1+3U_0/\omega)}\left(\frac{1+\cos(\pi/K)}{1-\cos(\pi j/K)}\right), \tag{5.8a}$$

where $\mathcal{D}_{0,c}$ is given by

$$\mathcal{D}_{0,c} \equiv \frac{\omega^3 S}{8\pi^2\alpha^2 K^4\,(1+\cos(\pi/K))}\left(1+\frac{3U_0}{\omega}\right). \tag{5.8b}$$

We observe that when $j = K-1$, we have $D^+_{0,j} = \mathcal{D}_{0,c}$. Now since $D_j/D^\star_{\rm low} = \mathcal{D}_0/D^-_{0,j}$, the Hopf bifurcation threshold in (5.5) becomes

$$\hat\tau_{uH,j} = \mathcal{H}\left(\mathcal{D}_0/D^-_{0,j}\right), \qquad \text{on} \quad D^-_{0,j} < \mathcal{D}_0 < D^+_{0,j}\,. \tag{5.9}$$

At the left-end of the interval we readily calculate the limiting behavior that $\hat\tau_{uH,j} \sim \mathcal{O}\left(\left(\mathcal{D}_0/D^-_{0,j}-1\right)^{-1}\right)$ as $\mathcal{D}_0 \to D^-_{0,j}$ from above. At the right end of the interval we have that

$$\hat\tau_{uH_j} \sim \frac{\omega\alpha}{6U_0}\left(\frac{U_0}{\omega}+1\right)\left(\frac{3U_0}{\omega}+1\right), \quad \text{as} \quad \mathcal{D}_0 \to D^+_{0,j}\,, \tag{5.10}$$

which is independent of j.

For each fixed $j = 1,\ldots,K-1$, we summarize the behavior of the roots of the quadratic (3.35), corresponding to the discrete eigenvalues of the NLEP (3.37) as follows:

Proposition 5.1 *For each fixed $j = 1,\ldots,K-1$, let λ_+ and λ_-, with $Re(\lambda_+) \ge Re(\lambda_-)$, denote the two solutions of the quadratic equation (3.35). Then, their location in the complex plane depends on $\mathcal{D}_0$ and $\hat\tau_u$ as follows:*

- *For $\mathcal{D}_0 > D^+_{0,j}$, we have $\lambda_+ > 0$ and $\lambda_- < 0$ for all $\hat\tau_u \ge 0$.*
- *For $\mathcal{D}_0 < D^-_{0,j}$, we have $Re(\lambda_\pm) < 0$ for all $\hat\tau_u \ge 0$.*
- *For $D^-_{0,j} < \mathcal{D}_0 < D^+_{0,j}$ we have $Re(\lambda_\pm) > 0$ when $\hat\tau_u > \hat\tau_{uH,j}$ and $Re(\lambda_\pm) < 0$ when $0 \le \hat\tau_{uH,j} < \hat\tau_u$.*

Here the Hopf bifurcation threshold $\hat\tau_{uH,j}$, which is defined on the interval $D^-_{0,j} < \mathcal{D}_0 < D^+_{0,j}$, is given in (5.9).

Since $D^+_{0,j}/D^-_{0,j} = 1 + 3U_0/\omega$, we observe that the width of the interval $D^-_{0,j} < \mathcal{D}_0 < D^+_{0,j}$ where an asynchronous oscillatory instability in the hotspot amplitudes is nonzero only as a result of the simple coupling term $-U$ in our three-component RD system (1.1). In the absence of police, this interval disappears and the basic crime model does not support oscillatory instabilities in this parameter regime.

Next, we examine the monotonicity properties of the universal function $\mathcal{H}(\beta)$ characterizing Hopf bifurcations, as defined in (5.5b), on the interval $1 < \beta < D^+_{0,j}/D^-_{0,j} = 1 + 3U_0/\omega$. We calculate $\mathcal{H}'(\beta)$ to get

$$\mathcal{H}'(\beta) = \frac{\alpha}{6(\beta-1)^2}\left[(\beta-1)^2 - 3\right],$$

so that $\mathcal{H}'(\beta) < 0$ if $1 < \beta < 1+\sqrt{3}$ and $\mathcal{H}'(\beta) > 0$ if $\beta > 1+\sqrt{3}$. We conclude that $\mathcal{H}'(\beta) < 0$ on $1 < \beta < 1 + 3U_0/\omega$ only when $\omega > \sqrt{3}U_0$. Since $\omega = S(\gamma-\alpha) - U_0$ we conclude that

$$\mathcal{H}'(\beta) < 0 \quad \text{on} \quad 1 < \beta < 3U_0/\omega\,, \quad \text{iff} \quad U_0 < \frac{S(\gamma-\alpha)}{1+\sqrt{3}}\,. \tag{5.11}$$

If $\frac{S(\gamma-\alpha)}{1+\sqrt{3}} < U_0 < U_{0,\max}$, then $\mathcal{H}(\beta)$ increases on $\sqrt{3} < \beta < 1 + 3U_0/\omega$.

Next, we rewrite the coefficients c_0, c_1, and c_2, in the quadratic (3.35) so as to readily calculate the Hopf bifurcation eigenvalue $\lambda = i\lambda_{IH}$. After some algebra we obtain that

$$c_0 = -\frac{1}{2}\left(1+\frac{3U_0}{\omega}\right)\left(\frac{\mathcal{D}_0}{D^+_{0,j}}-1\right), \qquad c_1 = \frac{\hat{\tau}_{uH,j}}{\alpha}\left(\frac{D^-_{0,j}}{\mathcal{D}_0}-1\right)\left(\frac{\hat{\tau}_u}{\hat{\tau}_{uH,j}}-1\right), \qquad c_2 = \frac{\hat{\tau}_{uH,j}}{3\alpha}\left(\frac{2D^-_{0,j}}{\mathcal{D}_0}+1\right), \tag{5.12}$$

where $\hat{\tau}_{uH,j}$ is defined in (5.9). The Hopf bifurcation eigenvalue $\lambda = i\lambda_{IH}$ with $\lambda_{IH} > 0$ is $\lambda_{IH} = \sqrt{c_0/c_2}$, which yields

$$\lambda_{IH} = \frac{3}{\left(2+\mathcal{D}_0/D^-_{0,j}\right)}\sqrt{\left(1+\frac{3U_0}{\omega}\right)\left(1-\frac{\mathcal{D}_0}{D^+_{0,j}}\right)\left(\frac{\mathcal{D}_0}{D^-_{0,j}}-1\right)}, \quad \text{on} \quad D^-_{0,j} < \mathcal{D}_0 < D^+_{0,j}\,. \tag{5.13}$$

This shows that λ_{IH} vanishes at both endpoints. We use the asymptotic behaviors $\mathcal{D}_0/D^+_{0,j} \to (1+3U_0/\omega)^{-1}$ as $\mathcal{D}_0 \to D^-_{0,j}$ and $\mathcal{D}_0/D^-_{0,j} \to (1+3U_0/\omega)$ as $\mathcal{D}_0 \to D^+_{0,j}$, so that from (5.13) we obtain the limiting asymptotic behavior

$$\lambda_{IH} \sim \frac{1}{(1+U_0/\omega)}\sqrt{\frac{3U_0}{\omega}\left(1+\frac{3U_0}{\omega}\right)\left(1-\frac{\mathcal{D}_0}{D^+_{0,j}}\right)} \quad \text{as} \quad \mathcal{D}_0 \to D^+_{0,j}\,; \qquad \lambda_{IH} \sim \sqrt{\frac{3U_0}{\omega}\left(\frac{\mathcal{D}_0}{D^-_{0,j}}-1\right)} \quad \text{as} \quad \mathcal{D}_0 \to D^-_{0,j}\,. \tag{5.14}$$

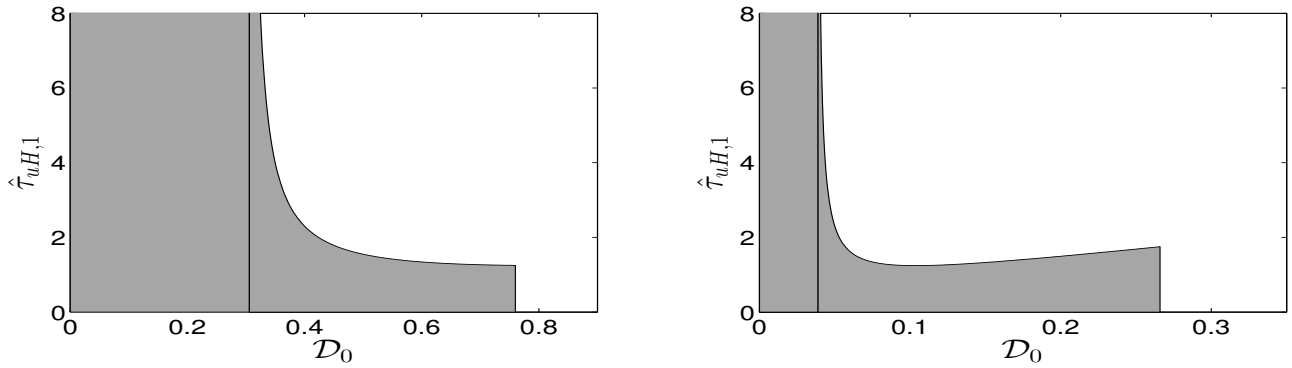

Figure 5: Plot of the Hopf bifurcation threshold $\hat{\tau}_{uH_1}$ versus $\mathcal{D}_0$ on the range $\mathcal{D}_{0,c}/(1+3U_0/\omega) < \mathcal{D}_0 < \mathcal{D}_{0c}$ for $K = 2$, $q = 3$, $S = 6$, $\gamma = 2$, $\alpha = 1$, and with $U_0 = 2$ (left panel) and $U_0 = 4$ (right panel). The shaded region is where the steady-state two-hotspot pattern is linearly stable. The thin vertical line in each figure is the lower boundary $\mathcal{D}_{0,c}/(1+3U_0/\omega)$, while the right edge of the shaded region is the competition stability threshold. The Hopf bifurcation curve in the right panel is not monotonic since $U_0 > S(\gamma-\alpha)/(1+\sqrt{3})$ when $U_0 = 4$.

For the special case $K = 2$, we now state our main result stability result related to Hopf bifurcations.

Proposition 5.2 *For $\epsilon \to 0$, $U_0 > 0$, $q = 3$, $\hat{\tau}_u \ll \mathcal{O}(\epsilon^{-2})$, and $\mathcal{D}_0 = \epsilon^2 D = \mathcal{O}(1)$, the linear stability properties of a two-hotspot steady-state solution of (1.6) are as follows:*

- *For $\mathcal{D}_0 > D^+_{0,1} \equiv \mathcal{D}_{0,c}$, the NLEP (3.37) has a positive real eigenvalue for all $\hat{\tau}_u \geq 0$ and so the two-hotspot steady-state is unstable. Here $\mathcal{D}_{0,c} = S\omega^3\left(1+3U_0/\omega\right)/[128\pi^2\alpha^2]$ is the competition stability threshold with $\omega \equiv S(\gamma-\alpha) - U_0$.*

- *On the range $D^-_{0,1} \equiv \mathcal{D}_{0,c}/\left(1+3U_0/\omega\right) < \mathcal{D}_0 < \mathcal{D}_{0,c}$, there is a Hopf bifurcation of the spot amplitudes when*

$$\hat{\tau}_u \equiv \hat{\tau}_{uH,1} = \mathcal{H}\left(\mathcal{D}_0/D^-_{0,1}\right), \quad \text{on} \quad D^-_{0,1} < \mathcal{D}_0 < \mathcal{D}_{0,c}\,, \tag{5.15}$$

  where $\mathcal{H}(\beta)$ is defined in (5.5b). When $\hat{\tau}_u > \hat{\tau}_{uH,1}$, the two-hotspot steady-state is unstable, while if $\hat{\tau}_u < \hat{\tau}_{uH,1}$ the two-hotspot pattern is linearly stable.

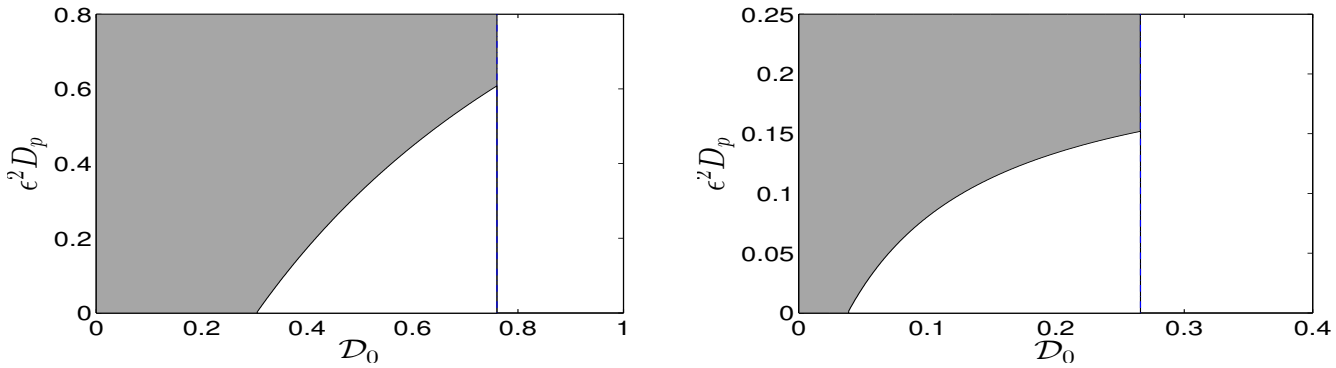

Figure 6: Plot of the Hopf bifurcation threshold for the scaled police diffusivity $\epsilon^2 D_p \equiv \mathcal{D}_0/\hat{\tau}_{uH_1}$ versus $\mathcal{D}_0$ on the range $\mathcal{D}_{0,c}/(1+3U_0/\omega) < \mathcal{D}_0 < \mathcal{D}_{0c}$ for $K = 2$, $q = 3$, $S = 6$, $\gamma = 2$, $\alpha = 1$, and with $U_0 = 2$ (left panel) and $U_0 = 4$ (right panel). The thin vertical line in each figure is the competition stability threshold $\mathcal{D}_{0,c}$ given in Proposition 5.2. The shaded region is where the steady-state two-hotspot pattern is linearly stable. For $\mathcal{D}_0 > \mathcal{D}_{0c}$ the hotspot solution is unstable due to a competition instability, whereas in the small unshaded region for $\mathcal{D}_0 < \mathcal{D}_{0c}$, the hotspot steady-state is unstable to an asynchronous oscillatory instability of the hotspot amplitudes.

- *On the range $0 < \mathcal{D}_0 < D_{0,1}^- \equiv \mathcal{D}_{0,c}/(1+3U_0/\omega)$, the two-hotspot steady-state is linearly stable for all $\hat{\tau}_u \geq 0$.*

In terms of a scaled police diffusivity defined by $\epsilon^2 D_p \equiv \mathcal{D}_0/\hat{\tau}_u$, Proposition 5.2 implies the following:

Corollary 5.3 *Under the conditions of Proposition 5.2 we have the following:*

- *For $\mathcal{D}_0 > \mathcal{D}_{0,c} \equiv S\omega^3(1+3U_0/\omega)/[128\pi^2\alpha^2]$, the two-hotspot steady-state is unstable for all scaled police diffusivities $\epsilon^2 D_p > 0$.*
- *On the range $\mathcal{D}_{0,c}/(1+3U_0/\omega) < \mathcal{D}_0 < \mathcal{D}_{0,c}$, the two hotspot steady-state is unstable to an asynchronous oscillatory instability of the hotspot amplitudes if $\epsilon^2 D_p < \mathcal{D}_0/\hat{\tau}_{uH,1}$, while the steady-state is linearly stable when $\epsilon^2 D_p > \mathcal{D}_0/\hat{\tau}_{uH,1}$. Here $\hat{\tau}_{uH,1}$ is the Hopf bifurcation threshold in (5.15).*
- *On the range $0 < \mathcal{D}_0 < \mathcal{D}_{0,c}/(1+3U_0/\omega)$, the two-hotspot steady-state is linearly stable for all $\epsilon^2 D_p \geq 0$.*

We now illustrate our main stability results for $K = 2$, $S = 6$, $\gamma = 2$, and $\alpha = 1$. In Fig. 5 we plot the region of linear stability in the $\hat{\tau}_u$ versus $\mathcal{D}_0$ parameter plane for $U_0 = 2$ (left panel) and $U_0 = 4$ (right panel). For $U_0 = 4$, we have $\omega < \sqrt{3}U_0$, and so the Hopf bifurcation threshold $\hat{\tau}_{uH,1}$ is not monotonic in $\mathcal{D}_0$, as seen in the right panel of Fig. 5. From this figure, we observe that as U_0 increases the region where the two-hotspot steady-state is linearly stable is smaller, as expected. With regards to the scaled police diffusivity $\epsilon^2 D_p \equiv \mathcal{D}_0/\hat{\tau}_u$, in Fig. 6 we plot the corresponding region of linear stability in the D_p versus $\mathcal{D}_0$ plane. In §5.2 we discuss this result qualitatively and compare the predicted stability threshold against full numerical solutions of the PDE system (1.6).

5.1 The Stability Phase Diagram for $q = 3$: $K \geq 3$ Hotspots

Next, we determine the parameter range of $\mathcal{D}_0$ and $\hat{\tau}_u$ for which a K-hotspot steady-state solution, with $K \geq 3$, is linearly stable. To do so, we need to guarantee that $\mathrm{Re}(\lambda) < 0$ for each of the quadratics in (3.35), i.e. for each $j = 1, \ldots, K-1$. In this way, we will ensure that any discrete eigenvalue of the NLEP (3.37) satisfies $\mathrm{Re}(\lambda) \leq 0$.

By using (5.8), we readily obtain the ordering principle that

$$D_{0,j+1}^{\pm} < D_{0,j}^{\pm}\,, \quad \text{and} \quad D_{0,j}^{-} < D_{0,j}^{+}\,, \qquad \text{for} \quad j = 1, \ldots, K-3\,. \tag{5.16}$$

We conclude that

$$D^+_{0,K-1} = \min_{j=1,\ldots,K-2}\{D^+_{0,j}\}\,, \qquad D^-_{0,K-1} = \min_{j=1,\ldots,K-2}\{D^-_{0,j}\}\,. \tag{5.17}$$

From Proposition 5.1, we conclude for each of the quadratics (3.35), i.e. for each $j = 1,\ldots,K-1$, that $\mathrm{Re}(\lambda) < 0$ for any $\hat{\tau}_u \geq 0$ when $\mathcal{D}_0 < D^-_{0,K-1}$. Therefore, a K-hotspot steady-state pattern is linearly stable for all $\hat{\tau}_u \geq 0$ on the range $0 < \mathcal{D}_0 < D^-_{0,K-1}$. For the range $\mathcal{D}_0 > D^+_{0,K-1}$, we conclude from Proposition 5.1 that the $K-1$ mode must be unstable due to a positive real eigenvalue for any $\hat{\tau}_u \geq 0$. Therefore, for $\mathcal{D}_0 > D^+_{0,K-1}$, a K-hotspot steady-state solution is unstable for all $\hat{\tau}_u \geq 0$. Additional unstable eigenvalues due to Hopf bifurcations associated with the modes $j = 1,\ldots,K-2$ are possible depending on the value of $\hat{\tau}_u$.

To complete the stability phase diagram in the $\hat{\tau}_u$ versus $\mathcal{D}_0$ parameter plane, we need only focus on the interval $D^-_{0,K-1} < \mathcal{D}_0 < D^+_{0,K-1}$. On this interval, the sign-alternating $K-1$ mode undergoes a Hopf bifurcation at $\hat{\tau}_u = \hat{\tau}_{uH,K-1}$, as given from (5.9) by

$$\hat{\tau}_{uH,K-1} \equiv \mathcal{H}\,(\beta)\,, \qquad \text{on} \quad 1 \leq \beta \leq \frac{D^+_{0,K-1}}{D^-_{0,K-1}} = 1 + \frac{3U_0}{\omega}\,, \qquad \text{where} \quad \beta \equiv \frac{\mathcal{D}_0}{D^-_{0,K-1}}\,. \tag{5.18}$$

Here $\mathcal{H}(\beta)$ is defined in (5.5b). When $\hat{\tau}_u > \hat{\tau}_{uH,K-1}$ the $K-1$ mode is unstable, whereas if $\hat{\tau}_u < \hat{\tau}_{uH,K-1}$ the $K-1$ mode is linearly stable.

We now seek to determine conditions for which the Hopf bifurcation threshold for the $K-1$ mode is smaller than any of the other $K-2$ possible Hopf bifurcation values $\hat{\tau}_{uH,j}$ for $j = 1,\ldots,K-2$ when restricted to the interval $D^-_{0,K-1} < \mathcal{D}_0 < D^+_{0,K-1}$. From (5.9), these other Hopf bifurcation thresholds, for $j = 1,\ldots,K-2$, can be written in terms of β, as defined in (5.18), by

$$\hat{\tau}_{uH,j} = \mathcal{H}(\xi_j\beta)\,, \qquad \text{on} \quad \frac{1}{\xi_j} \leq \beta \leq \frac{1}{\xi_j}\left(1 + \frac{3U_0}{\omega}\right)\,, \tag{5.19a}$$

where, from (5.8), we define

$$\xi_j \equiv \frac{D^-_{0,K-1}}{D^-_{0,j}} = \frac{1-\cos\left(\pi j/K\right)}{1+\cos\left(\pi/K\right)}\,, \qquad j = 1,\ldots,K-2\,. \tag{5.19b}$$

Since $\xi_{K-1} = 1$, (5.19b) reduces to (5.18) if we set $j = K-1$. We observe from (5.19b) that the following ordering principle holds:

$$\xi_j < \xi_{j+1} < 1\,, \qquad j = 1,\ldots,K-3\,, \qquad \xi_{K-2} = \max_{j=1,\ldots,K-2}\{\xi_j\}\,. \tag{5.19c}$$

Comparing the intervals in (5.19a) and (5.18), we want to determine a specific parameter range of the total police deployment U_0 for which, for any $j = 1,\ldots,K-2$, we have that $\hat{\tau}_{uH,K-1} < \hat{\tau}_{uH,j}$ on the overlap domain $\xi_j^{-1} \leq \beta \leq 1+3U_0/\omega$. If the overlap domain is the null-set for the j-th mode, i.e. if $\xi_j < 1/(1+3U_0/\omega)$, then we can simply ignore the j-th mode on $D^-_{0,K-1} < \mathcal{D}_0 < D^+_{0,K-1}$. As such, we need only consider values of j (if any) for which $\xi_j^{-1} < 1 + 3U_0/\omega$, so that an overlap domain exists. Since $\mathcal{H}(\beta)$ is monotone decreasing on $1 < \beta < 1+\sqrt{3}$, we readily obtain that $\mathcal{H}(\beta) - \mathcal{H}(\xi_j\beta) \equiv \int_{\xi_j\beta}^{\beta} \mathcal{H}'(\eta)\,d\eta < 0$ on the interval $\xi_j^{-1} < \beta < 1+\sqrt{3}$. In this way, we conclude that

$$\mathcal{H}(\xi_j\beta) < \mathcal{H}(\beta)\,, \qquad \text{on} \quad \xi_j^{-1} \leq \beta \leq 1 + \frac{3U_0}{\omega}\,, \qquad \text{when} \quad \omega > \sqrt{3}U_0\,. \tag{5.20}$$

Therefore, on the range for which $\mathcal{H}(\beta)$ is monotonically decreasing, it follows that the Hopf bifurcation threshold of $\hat{\tau}_u$ for any mode $j = 1,\ldots,K-2$ cannot be smaller than that for the $K-1$ mode. Although the monotonicity of $\mathcal{H}(\beta)$ on the range $\xi_j^{-1} \leq \beta \leq 1 + 3U_0/\omega$ for $\omega > \sqrt{3}U_0$ provides a sufficient condition for the ordering principle $\hat{\tau}_{uH,K-1} < \hat{\tau}_{uH,j}$

for $j = 1, \ldots, K-2$ to hold, we now show from a more detailed calculation that the monotonicity of $\mathcal{H}(\beta)$ is not strictly necessary.

We now determine a precise condition that ensures that $\hat{\tau}_{uH,K-1} < \hat{\tau}_{uH,K-2}$ on an assumed overlap domain $\xi_{K-2}^{-1} \leq \beta \leq 1 + 3U_0/\omega$. Owing to the ordering principle $\xi_j < \xi_{j+1}$ for $j = 1, \ldots, K-3$ from (5.19c), the first Hopf threshold to potentially decrease below that of the $K-1$ mode must be the $K-2$ mode, and so we focus only on a comparison with the $K-2$ mode. From (5.18) and (5.19a), and by using the explicit expression for $\mathcal{H}(\beta)$ in (5.5b), we calculate after some algebra that $\mathcal{H}(\xi_{K-2}\beta) \geq \mathcal{H}(\beta)$ on $\xi_{K-2}^{-1} \leq \beta \leq 1 + 3U_0/\omega$, if and only if

$$\mathcal{K}(\beta) \equiv (\xi_{K-2}\beta - 1)(\beta - 1) < 3\,, \qquad \text{on} \quad 1 < \xi_{K-2}^{-1} \leq \beta \leq 1 + 3U_0/\omega\,. \tag{5.21}$$

Since $\mathcal{K}'(\beta) > 0$ on this interval, this inequality holds if and only if $1 + \frac{3U_0}{\omega} < \beta_{\max}$, where $\mathcal{K}(\beta_{\max}) = 3$. By setting $\mathcal{K}(\beta) = 3$, and solving the quadratic for $\beta = \beta_{\max}$, we obtain that (5.21) holds if and only if

$$\frac{\sqrt{3}U_0}{\omega} < \mathcal{Z}(\xi_{K-2})\,, \qquad \text{where} \quad \mathcal{Z}(\xi_{K-2}) \equiv \frac{1}{\sqrt{3}}\left(-\frac{1}{2} + \frac{1}{2\xi_{K-2}}\left[1 + \sqrt{\xi_{K-2}^2 + 10\xi_{K-2} + 1}\right]\right). \tag{5.22}$$

Here $\omega = S(\gamma - \alpha) - U_0$ and ξ_{K-2} can be found from (5.19b). On $0 < \xi < 1$, we have that $\mathcal{Z}(\xi)$ satisfies

$$\mathcal{Z}(\xi) \to +\infty \quad \text{as} \quad \xi \to 0^+\,, \qquad \mathcal{Z}(1) = 1\,, \qquad \mathcal{Z}'(\xi) < 0\,, \quad \text{on} \quad 0 < \xi < 1 \tag{5.23}$$

It follows that $\mathcal{Z}(\xi) > 1$ on $0 < \xi < 1$. The key inequality (5.22) implies that $\omega > \sqrt{3}U_0/\mathcal{Z}(\xi_{K-2})$, which yields a larger range of ω than the range $\omega > \sqrt{3}U_0$ where $\mathcal{H}(\beta)$ is monotonic. This inequality (5.22) can also be used to give a precise upper bound on U_0 for which the $K-1$ mode determines the Hopf bifurcation threshold for $\hat{\tau}_u$ on the entire range $D_{0,K-1}^- < \mathcal{D}_0 < D_{0,K-1}^+$.

In this way, for $K \geq 3$ we summarize our main stability result for a K-hotspot steady-state solution as follows:

Proposition 5.4 *For $\epsilon \to 0$, $U_0 > 0$, $q = 3$, $K \geq 3$, $\hat{\tau}_u \ll \mathcal{O}(\epsilon^{-2})$, and $\mathcal{D}_0 = \epsilon^2 D = \mathcal{O}(1)$, the linear stability properties of a K-hotspot steady-state solution of (1.6) are as follows:*

- *For $\mathcal{D}_0 > D_{0,K-1}^+ \equiv \mathcal{D}_{0,c}$, the NLEP (3.37) has at least one positive real eigenvalue for all $\hat{\tau}_u \geq 0$. Additional unstable eigenvalues as a result of Hopf bifurcations associated with the other modes $j = 1, \ldots, K-2$ are possible depending on the value of $\hat{\tau}_u$. Here $\mathcal{D}_{0,c}$ is the competition stability threshold given in (4.9) with $q = 3$.*

- *On the range $D_{0,K-1}^- \equiv \mathcal{D}_{0,c}/(1 + 3U_0/\omega) < \mathcal{D}_0 < \mathcal{D}_{0,c}$, and when U_0 satisfies*

$$U_0 < U_{0,swit} \equiv \left(\frac{\mathcal{Z}(\xi_{K-2})}{\sqrt{3} + \mathcal{Z}(\xi_{K-2})}\right) S(\gamma - \alpha)\,, \qquad \textit{where} \quad \xi_{K-2} \equiv \frac{1 - \cos(\pi(K-2)/K)}{1 + \cos(\pi/K)}\,, \tag{5.24}$$

  and where $\mathcal{Z}(\xi)$ is defined in (5.22), the $K-1$ sign-alternating mode sets the stability threshold on the entire range. For $\hat{\tau}_u > \hat{\tau}_{uH,K-1}$, the K-hotspot pattern is unstable, while if $\hat{\tau}_u < \hat{\tau}_{uH,K-1}$ the K-hotspot pattern is linearly stable. This smallest Hopf bifurcation threshold value of $\hat{\tau}_u$ is defined by

$$\hat{\tau}_{uH,K-1} \equiv \mathcal{H}\left(\mathcal{D}_0/D_{0,K-1}^-\right), \quad \textit{on} \quad D_{0,K-1}^- \equiv \frac{\mathcal{D}_{0c}}{1 + 3U_0/\omega} < \mathcal{D}_0 < \mathcal{D}_{0,c}\,, \tag{5.25}$$

  where $\mathcal{H}(\beta)$ is defined in (5.5b).

- *On the range $0 < \mathcal{D}_0 < D_{0,K-1}^- \equiv \mathcal{D}_{0,c}/(1 + 3U_0/\omega)$, the K-hotspot steady-state is linearly stable for all $\hat{\tau}_u \geq 0$.*

In terms of a scaled police diffusivity defined by $\epsilon^2 D_p \equiv \mathcal{D}_0/\hat{\tau}_u$, Proposition 5.4 implies the following:

Corollary 5.5 *Under the conditions of Proposition 5.4, we have the following:*

- *For $\mathcal{D}_0 > \mathcal{D}_{0,c}$, the K-hotspot steady-state is unstable for all scaled police diffusivities $\epsilon^2 D_p > 0$. Here $\mathcal{D}_{0,c}$ is defined in (4.9) with $q = 3$.*

- *On the range $\mathcal{D}_{0,c}/\left(1 + 3U_0/\omega\right) < \mathcal{D}_0 < \mathcal{D}_{0,c}$, and when $U_0 < U_{0,swit}$, as defined in (5.24), the K-hotspot steady-state is unstable to a sign-alternating asynchronous oscillatory instability of the hotspot amplitudes if $\epsilon^2 D_p < \mathcal{D}_0/\hat{\tau}_{uH,K-1}$ where $\hat{\tau}_{uH,K-1}$ is defined in (5.25). Alternatively, this steady-state is linearly stable when $\epsilon^2 D_p > \mathcal{D}_0/\hat{\tau}_{uH,K-1}$.*

- *On the range $0 < \mathcal{D}_0 < \mathcal{D}_{0,c}/\left(1 + 3U_0/\omega\right)$, the K-hotspot steady-state is linearly stable for all $\epsilon^2 D_p \geq 0$.*

We remark that the upper bound $U_{0,\text{swit}}$ in (5.24) can be calculated explicitly when $K = 3$ and $K = 4$. When $K = 3$, we calculate $\xi_1 = 1/3$ and $\mathcal{Z}(\xi_1) = \left(1 + \sqrt{10}\right)/\sqrt{3}$. We then obtain from (5.24) that the sign-alternating $K - 1$ mode sets the Hopf bifurcation threshold when

$$U_0 < U_{0,\text{swit}} \equiv \frac{3}{2 + \sqrt{10}} S(\gamma - \alpha) \approx (0.58114) S(\gamma - \alpha)\,, \qquad \text{for} \quad K = 3\,. \tag{5.26}$$

Similarly, for $K = 4$, we calculate $\xi_2 = 2 - \sqrt{2}$, and

$$\mathcal{Z}(\xi_2) = \frac{1}{\sqrt{3}} \left[\frac{\sqrt{2}}{4} + \left(\frac{1}{2} + \frac{\sqrt{2}}{4} \right) \sqrt{27 - 14\sqrt{2}} \right] \approx 1.5265\,.$$

From (5.24), the $K - 1$ mode sets the Hopf bifurcation threshold when

$$U_0 < U_{0,\text{swit}} \approx (0.46847) S(\gamma - \alpha)\,, \qquad \text{for} \quad K = 4\,. \tag{5.27}$$

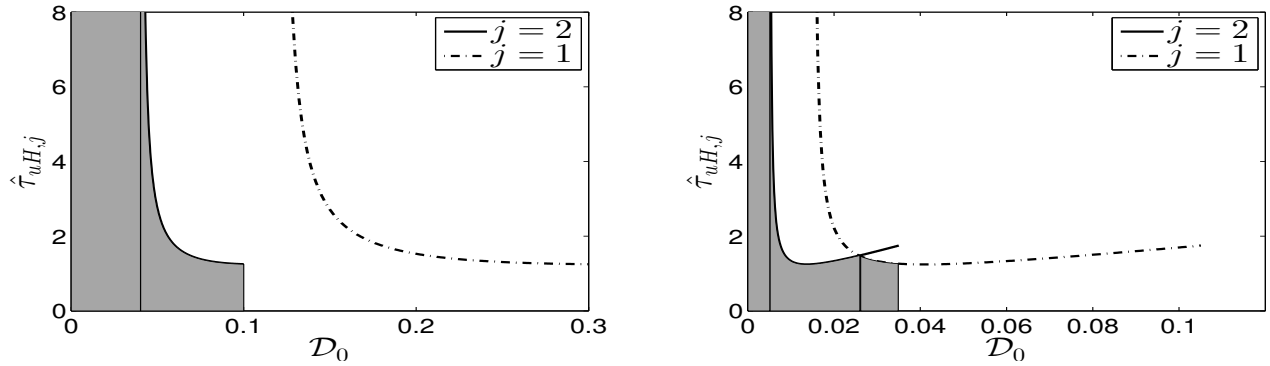

Figure 7: Linear stability (shaded) region in the $\hat{\tau}_u$ versus $\mathcal{D}_0$ plane for $K = 3$ when $S = 6$, $\gamma = 2$, and $\alpha = 1$, and for $U_0 = 2$ (left panel) and $U_0 = 4$ (right panel), as characterized by Proposition 5.4. To the left of the thin vertical line the steady-state is unconditionally stable. The solid and dot-dashed curves are the Hopf bifurcation boundaries for the (sign-alternating) $j = 2$ mode and the $j = 1$ mode, respectively. For $U_0 = 2$ (left panel) the Hopf boundary is determined by the $j = 2$ mode. For $U_0 = 4 > U_{0,swit} \approx 3.478$ (right panel) the Hopf boundary consists of both the $j = 2$ and $j = 1$ mode. The three-hotspot steady-state is unstable to an oscillatory instability above the solid or dotted curves. At the ends of the Hopf bifurcation curves the Hopf eigenvalue tends to zero.

We now illustrate our main stability results in Proposition 5.4 and Corollary 5.5 for either $S = 6$, $\gamma = 2$, and $\alpha = 1$. We take $K = 3$ or $K = 4$, and either $U_0 = 2$ and $U_0 = 4$. For these parameters, (5.26) and (5.27) yield that $U_{0,\text{swit}} \approx 3.487$ for $K = 3$ and $U_{0,\text{swit}} \approx 2.811$ for $K = 4$. Therefore, for both $K = 3$ and $K = 4$ it is only for the smaller value $U_0 = 2$ that the sign-alternating mode sets the Hopf bifurcation threshold.

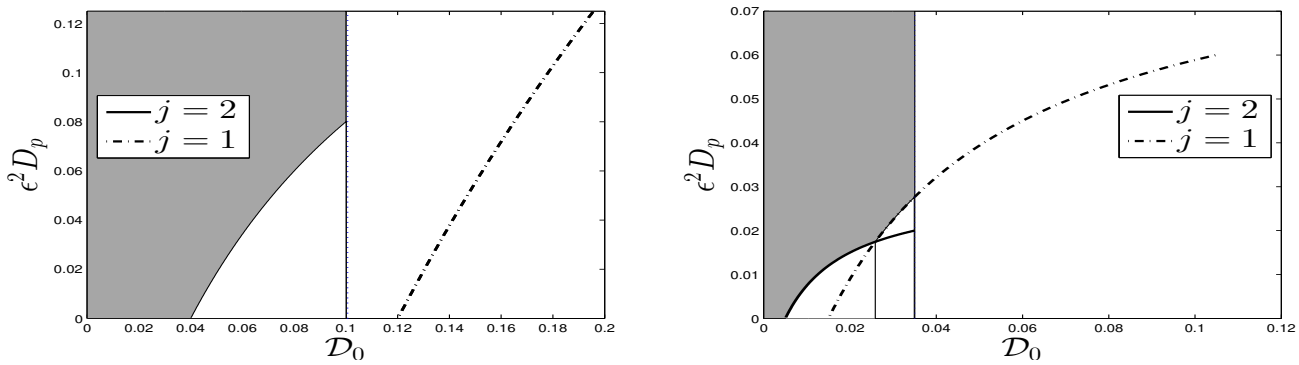

Figure 8: Same plot as Fig. 7 except in the scaled police diffusivity $\epsilon^2 D_p = \mathcal{D}_0/\hat{\tau}_u$ versus $\mathcal{D}_0$ plane for $K = 3$, $S = 6$, $\gamma = 2$, and $\alpha = 1$, with $U_0 = 2$ (left panel) and $U_0 = 4$ (right panel) (see Corollary 5.5). The three-hotspot steady-state is linearly stable in the shaded region. This steady-state undergoes an oscillatory instability below the solid or dot-dashed curves. In the left panel the thin vertical line is the competition threshold $\mathcal{D}_{0,c}$. The additional thin vertical line in the right panel is where the Hopf boundary switches from $j = 2$ to $j = 1$. This switch occurs since $U_0 = 4 > U_{0,swit} \approx 3.478$ (see (5.26) and the second statement of Corollary 5.5).

For $K = 3$, in Fig. 7 the shaded region is the theoretically predicted region of linear stability in the $\hat{\tau}_u$ versus $\mathcal{D}_0$ parameter plane for $U_0 = 2$ (left panel) and for $U_0 = 4$ (right panel). In this figure the dotted curve and solid curves are the Hopf bifurcation thresholds for the $j = 1$ mode and the sign-alternating $j = 2$ mode. When $U_0 = 2$ (left panel), the sign-alternating mode sets the boundary of the region of stability, whereas for $U_0 = 4$ (right panel) both the $j = 1$ and $j = 2$ Hopf bifurcation thresholds determine the region of stability. The corresponding region of stability in the scaled police diffusivity $\epsilon^2 D_p$ versus $\mathcal{D}_0$ parameter plane is shown in Fig. 8.

Similar results for $K = 4$ and for $U_0 = 2$ and $U_0 = 4$ are shown in Fig. 9 in the $\hat{\tau}_u$ versus $\mathcal{D}_0$ plane and in Fig. 10 in the $\epsilon^2 D_p$ versus $\mathcal{D}_0$ plane. From the left panels of Fig. 9 and Fig. 10, the $j = K - 1 = 3$ sign-alternating mode always sets the Hopf bifurcation boundary. However, as seen in the right panels of Fig. 9 and Fig. 10, where $U_0 = 4 > U_{0,\text{swit}} \approx 2.811$, we observe that both the $j = 3$ and $j = 2$ modes determine the Hopf bifurcation boundary when $\mathcal{D}_0 < \mathcal{D}_{0,c}$.

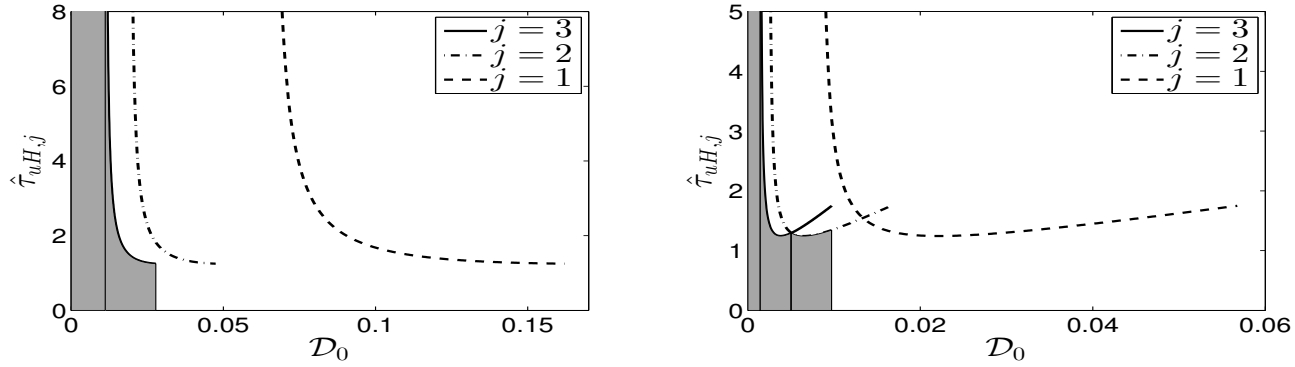

Figure 9: Linear stability (shaded) region in the $\hat{\tau}_u$ versus $\mathcal{D}_0$ plane for $K = 4$ when $S = 6$, $\gamma = 2$, and $\alpha = 1$, and for $U_0 = 2$ (left panel) and $U_0 = 4$ (right panel). The solid, dot-dashed, and dashed curves are the Hopf bifurcation boundaries for the (sign-alternating) $j = 3$ mode and the other $j = 2$ and $j = 1$ modes. For $U_0 = 2$ (left panel) the Hopf boundary is determined by the sign-alternating $j = 3$ mode. For $U_0 = 4 > U_{0,swit} \approx 2.811$ (see (5.27), the Hopf boundary consists of both the $j = 3$ and $j = 2$ mode. Oscillatory instabilities of the hotspot amplitudes occur above either the three Hopf bifurcation curves.

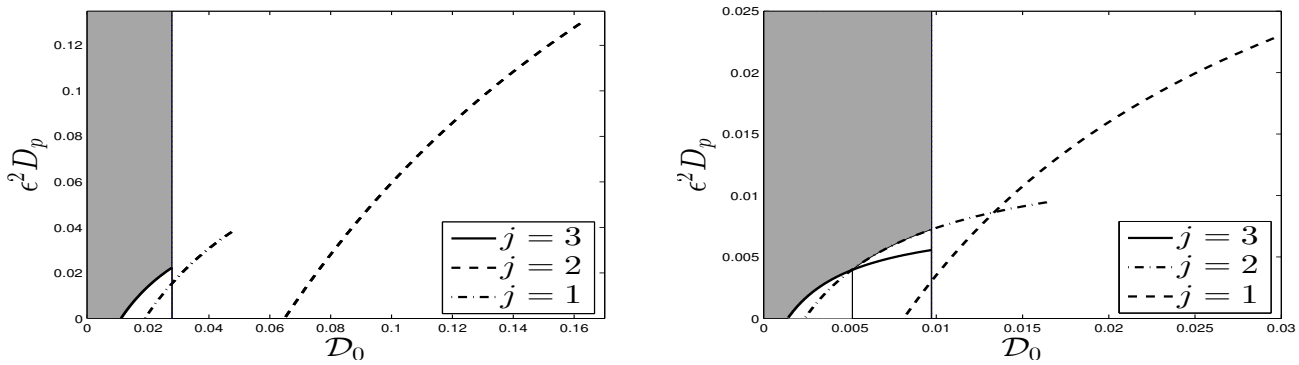

Figure 10: Plot corresponding to Fig. 9 in the scaled police diffusivity $\epsilon^2 D_p = \mathcal{D}_0/\hat{\tau}_u$ versus $\mathcal{D}_0$ plane for $K = 4$, $S = 6$, $\gamma = 2$, and $\alpha = 1$, with $U_0 = 2$ (left panel) and $U_0 = 4$ (right panel). The four-hotspot steady-state is linearly stable in the shaded region. This steady-state undergoes an oscillatory instability below either of the three Hopf bifurcation curves. In the left panel the thin vertical line is the competition threshold $\mathcal{D}_{0,c}$. The additional thin vertical line in the right panel is where the Hopf boundary switches from $j = 3$ to $j = 2$.

5.2 Numerical Validation: Asynchronous Oscillations $q = 3$

Here we discuss our main stability result qualitatively and we validate our Hopf bifurcation threshold values with full numerical solutions of the PDE system (1.6).

This section is to be written once I get the full numerics working. I might use some of the blurb below. This analysis reveals a qualitatively novel phenomenon in the context of the study of the stability of spike patterns to reaction-diffusion systems. In particular, for a two-hotspot equilibrium, then $j = 1$ is the only mode of oscillation, and our theory predicts the possibility of an *asynchronous* Hopf bifurcation so that the amplitudes of the two crime hotspots begin to exhibit temporal anti-phase oscillations. In terms of the urban crime model, this means that when police patrols with a certain specific diffusivity relative to the criminals (determined by $\tilde{\tau}_{j,\mathrm{Hopf}}$), one observes an interesting picture that the police concentration is drifting to and fro from the hotspots without annihilating any of them. However, if the police patrol diffusivity exceeds such a threshold, then one of the hotspot will dissipate due to an oscillatory instability. Such a qualitative behavior in the possible types of detstabilization of localized spike patterns was not observed in other well-studied reaction-diffusion systems exhibiting similar concentration phenomena, such as the Gray-Scott, Gierer-Meinhardt and Schnakenburg models.

6 Oscillatory Instabilities of the Hotspot Amplitudes: General $q \neq 3$

In this section we analyze the NLEP for the general case where $q \neq 3$.

Before we proceed, we would like to state a typical choice of model parameters, which we will use repeatedly in the subsequent figures for illustrating various stages of the analysis:

$$\alpha = 1\,, \quad \gamma = 2\,, \quad q = 2\,, \quad U_0 = 1\,, \quad \ell = 1\,, \quad K = 2\,, \quad j = 1\,, \quad S = 2K\ell = 4\,. \tag{6.1}$$

Our value $q = 2$ corresponds to the "cops on the dots" strategy, whereby the police patrol mimics that of the criminals.

6.1 The Starting and Ending Point of the Path and the Two Main Cases

The location of the end of the path at $\lambda_I = 0$ is easily determined. We have $\mathcal{F}(0) = 1/2$ from (**??**), and so

$$\zeta(0) = \zeta_R(0) = \mathcal{C}(0) - \frac{1}{2} = a(1 - \frac{b}{3}) - \frac{1}{2} \in \mathbb{R}\,.$$

Thus, the equation $\zeta(0) = 0$ corresponds to exactly $\mathcal{C}(0) = 1/2$, which we derived in (**??**) in Section **??** where we studied the competition instability threshold. Moreover, we conclude from (**??**) that

$$\zeta(0) > 0 \quad \text{when} \quad D_{j,2} > D_{j,2}^*\,; \qquad \zeta(0) < 0 \quad \text{when} \quad D_{j,2} < D_{j,2}^*\,.$$

Next, we consider the limiting behavior as $\lambda_I \to +\infty$. We begin by decomposing $\zeta(i\lambda_I)$ into real and imaginary parts as $\zeta(i\lambda_I) \equiv \zeta_R(\lambda_I) + i\zeta_I(\lambda_I)$. Then, we readily have the limiting behavior for $\zeta(i\lambda_I)$ as $\lambda_I \to \infty$, given by

$$\zeta(i\lambda_I) \sim a\,(1 + \tilde{\tau}_j b) + ia\tilde{\tau}_j\lambda_I \quad \text{as} \quad \lambda_I \to +\infty\,,$$

so that

$$\zeta_R(\lambda_I) \sim a(1 + \tilde{\tau}_j b), \qquad \zeta_I(\lambda_I) \sim a\tilde{\tau}_j\lambda_I\,, \quad \text{as} \quad \lambda_I \to \infty\,. \tag{6.2}$$

This means, with respect to the origin, that the path begins asymptotically close to the positive infinity of the imaginary axis.

Therefore, this reduces the problem to determining whether the path crosses the imaginary axis and real axis on the range $0 < \lambda_I < \infty$.

The easiest case to consider is for $D_{j,2} > D_{j,2}^*$ when the end point is on the positive real axis. Then, in order to prove

$$[\arg\zeta]|_{\Gamma_{I_+}} = -\frac{\pi}{2}\,,$$

it suffices to show that the path never crosses the imaginary axis. When this occurs we obtain that $N = 1$, which gives one unique unstable eigenvalue for the NLEP. Fig. 11 shows the path $\zeta(\Gamma_{I_+})$ in two distinctive cases.

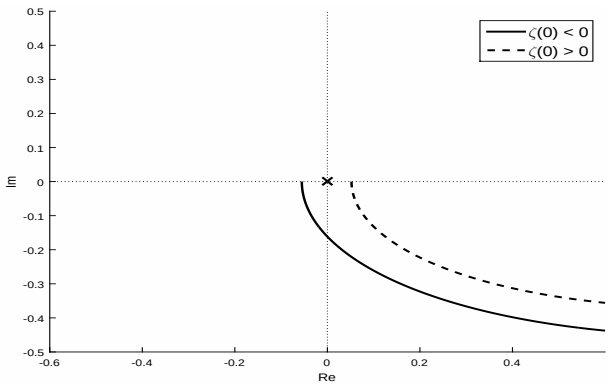

Figure 11: Close-up of two distinctive cases of the Nyquist plots for $K = 2$. For the model parameters stated in (6.1), and for $\tau_u = 1$, we show the Nyquist plot for two values of $\mathcal{D}_0$. The upper threshold, corresponding to the competition instability, is given by $\mathcal{D}_{0,upper} = \mathcal{D}_{0,1}^+ \approx 3.103$. The curve with $\zeta(0) < 0$ and $\zeta(0) > 0$ correspond to the choice $\mathcal{D}_0 = 3.0$ and $\mathcal{D}_0 = 3.2$, respectively. The number of unstable eigenvalues are respectively $N = 0$ and $N = 1$.

The next natural step would be to consider $D_{j,2} < D_{j,2}^*$, so that the end point is on the negative real axis. Then, by continuity, the imaginary axis must be crossed. If one can prove monotonicity in the real component it follows that there must be exactly one such crossing, and it would remain to determine whether it occurs on the positive or the negative imaginary axis. If it occurs on the positive imaginary axis, then it is clear that

$$[\arg\zeta]|_{\Gamma_{I_+}} = \frac{\pi}{2}\,,$$

so that $N = 2$, and we have two unstable eigenvalues. Otherwise, if it occurs on the negative imaginary axis, then

$$[\arg\zeta]|_{\Gamma_{I_+}} = -\frac{3\pi}{2}\,.$$

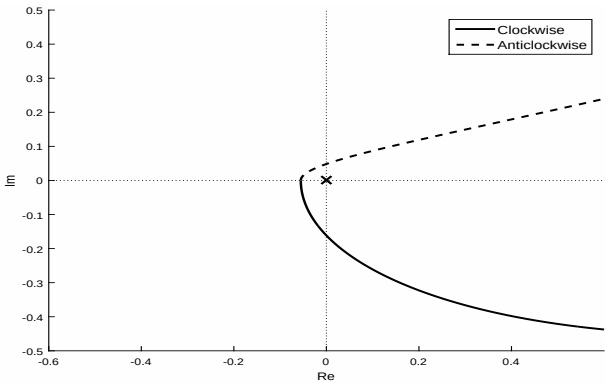

Figure 12: Close-up of two distinctive cases of Nyquist plots for $K = 2$. Parameter values common to both are $\alpha = 1$, $\gamma = 2$, $U_0 = 1$, $\mathcal{D}_0 = 3$ and $\ell = 1$ (but $S = 2K\ell = 4$). The curves that are clockwise and anticlockwise with respect to the origin correspond to the choices $\tau_u = 1$ and $\tau_u = 4$, respectively. The number of unstable eigenvalues are numerically determined to be $N = 0$ and $N = 2$ for these particular cases.

In this case we would have $N = 0$, and no unstable eigenvalues. See Fig. 12 for examples of both paths.

In order to distinguish between these two cases, we must determine detailed properties of the component functions $\mathcal{C}(\lambda)$ and $\mathcal{F}(\lambda)$, and especially for the latter, as it has no closed form representation.

Next we consider $\mathcal{C}(\lambda)$ restricted to the positive imaginary axis. We first separate $\mathcal{C}(i\lambda_I)$ into its real and imaginary parts as

$$\mathcal{C}(i\lambda_I) = a\,(1 + i\tilde{\tau}_j\lambda_I)\left(1 - \frac{b}{3 - i\lambda_I}\right) = a\,(1 + i\tilde{\tau}_j\lambda_I)\left(1 - \frac{b(3 + i\lambda_I)}{9 + \lambda_I^2}\right).$$

Therefore, if we denote $\mathcal{C}(i\lambda_I) = \mathcal{C}_R(\lambda_I) + i\mathcal{C}_I(\lambda_I)$, we have that

$$\mathcal{C}_R(\lambda_I) = a\left(1 + \tilde{\tau}_j b - \frac{3b}{9 + \lambda_I^2}\,(1 + 3\tilde{\tau}_j)\right), \tag{6.3a}$$

$$\mathcal{C}_I(\lambda_I) = \frac{a\lambda_I}{9 + \lambda_I^2}\left(3\tilde{\tau}_j\,(3 - b) - b + \tilde{\tau}_j\lambda_I^2\right). \tag{6.3b}$$

We now list several elementary properties of $\mathcal{C}_R(\lambda_I)$ and $\mathcal{C}_I(\lambda_I)$.

Properties of $\mathcal{C}_R(\lambda_I)$

(i) $\mathcal{C}_R(0) = a(1 - b/3)$. Therefore, $\mathcal{C}_R(0) > 0$ if and only if $b < 3$ (also, $\mathcal{C}_R(0) < 0$ if and only if $b > 3$). We also had earlier a similar condition that $\mathcal{C}_R(0) > 1/2$ if and only if $b - 3 + 3/(2a) < 0$, which occurs if and only if $D_{j,2} > D_{j,2}^*$.

(ii) $\mathcal{C}_R'(\lambda_I) > 0$ for $\lambda_I > 0$, and $\mathcal{C}_R(\lambda_I) \to a(1 + \tilde{\tau}_j b) > 0$ as $\lambda_I \to \infty$.

(iii) Suppose $b > 3$, then $\mathcal{C}_R(\lambda_I) < 0$ on the interval

$$0 < \lambda_I < \sqrt{\frac{3(b - 3)}{1 + \tilde{\tau}_j b}}.$$

Properties of $\mathcal{C}_I(\lambda_I)$

(iv) $\mathcal{C}_I(\lambda_I) \sim a\lambda_I\,[3\tilde{\tau}_j(3 - b) - b]$ as $\lambda_I \to 0^+$, and $\mathcal{C}_I(\lambda_I) \sim a\tilde{\tau}_j\lambda_I$ as $\lambda_I \to +\infty$.

(v) $\mathcal{C}_I(\lambda_I) < 0$ on $0 < \lambda_I^2 < 3(b - 3) + b/\tilde{\tau}_j$. Otherwise, we have $\mathcal{C}_I(\lambda_I) > 0$.

Therefore, if $b > 3/(1+\frac{1}{3\tilde{\tau}_j})$, it follows that there is a range of λ_I, given by

$$0 < \lambda_I < \sqrt{3(b-3) + \frac{b}{\tilde{\tau}_j}} \equiv \lambda_{I_I} \,,$$

for which $\mathcal{C}_I(\lambda_I) < 0$.

(vi) Alternatively if $b < 3/(1+\frac{1}{3\tilde{\tau}_j})$, we can then show that $\mathcal{C}_I(\lambda_I) > 0$ for all $\lambda_I > 0$.

To establish property (vi) above we begin by calculating

$$\mathcal{C}_I'(\lambda_I) = \frac{a}{(9+\lambda_I^2)^2}\left[\tilde{\tau}_j\lambda_I^4 + \lambda_I^2\left(18\tilde{\tau}_j + b + 3b\tilde{\tau}_j\right) + 9\left(\tilde{\tau}_j(9-3b) - b\right)\right] . \tag{6.4}$$

The expression in the brackets of 6.4 is a quadratic in $x = \lambda_I^2$, and upon setting $\mathcal{C}_I'(\lambda_I) = 0$, we see that the two roots $x_+ \geq x_-$ satisfy

$$x_+ + x_- = -\left[18\tilde{\tau}_j + b + 3b\tilde{\tau}_j\right]/\tilde{\tau}_j, \qquad x_+x_- = 9\left(\tilde{\tau}_j(9-3b) - b\right)/\tilde{\tau}_j \,.$$

Since $x_+ + x_- < 0$ always holds, there is a root $x_+ = \lambda_I^2 > 0$ if and only if $x_+x_- < 0$. It follows that there exists $\lambda_I^2 > 0$ for which $\mathcal{C}_I'(\lambda_I) = 0$ if and only if $\tilde{\tau}_j(9-3b) - b < 0$, which implies that $b > 3/(1+\frac{1}{3\tilde{\tau}_j})$ must hold. Therefore, $\mathcal{C}_I'(\lambda_I) > 0$ for any $\lambda_I > 0$, and with the fact that $\mathcal{C}_I(0) = 0$, we conclude $\mathcal{C}_I(\lambda_I) > 0$ always holds as well. This establishes property (v) for $\mathcal{C}_I(\lambda_I)$.

In Fig. 13 we show various plots of $\mathcal{C}_R(\lambda_I)$ and $\mathcal{C}_I(\lambda_I)$ for $\tau_u = 1$ and for the model parameters given in (6.1). These plots illustrate our established properties for $\mathcal{C}_R(\lambda_I)$ and $\mathcal{C}_I(\lambda_I)$.

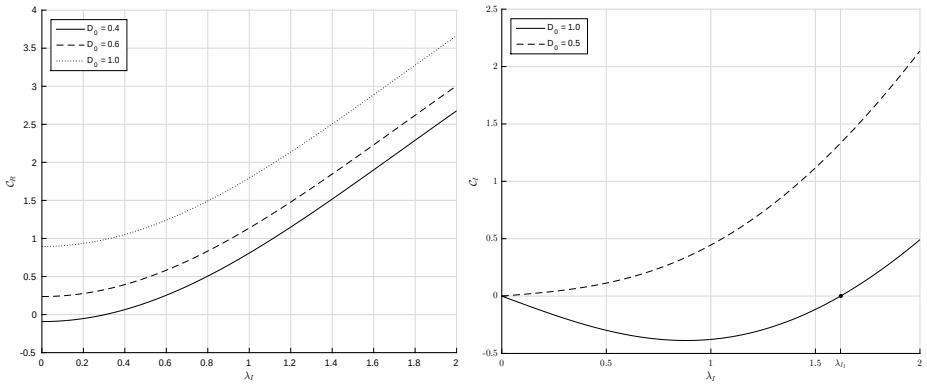

(a) (b)

Figure 13: Plots of $\mathcal{C}_R$ and $\mathcal{C}_I$ for $\tau_u = 1$ and the model parameters given in (6.1). The value for $\mathcal{D}_0$ was chosen as follows for each curve: Left figure: three cases of $\mathcal{C}_R(\lambda_I)$ are plotted: (i) $b > 3$ ($\mathcal{D}_0 = 0.4$), (ii) $3 - 3/(2a) < b < 3$ ($\mathcal{D}_0 = 0.6$), (iii) $b < 3 - 3/(2a)$ ($\mathcal{D}_0 = 1.0$). Right figure: two cases of $\mathcal{C}_I(\lambda_I)$ are plotted: (i) $b < 3/\left(1 + 1/(3\tilde{\tau}_j)\right)$ ($\mathcal{D}_0 = 1.0$), $b > 3/\left(1 + 1/(3\tilde{\tau}_j)\right)$ ($\mathcal{D}_0 = 0.5$), and the right end point of the interval of negative values for $\mathcal{C}_I$ is at $\lambda_{I_I} \approx 1.6204$, indicated by a heavy dot.

From property (ii) of $\mathcal{C}_R(\lambda_I)$ we have $\mathcal{C}_R'(\lambda_I) > 0$, while from property (ii) of $\mathcal{F}_R(\lambda_I)$ we conclude that $\mathcal{F}_R'(\lambda_I) < 0$. Therefore, we have that $\zeta_R(\lambda_I) = \mathrm{Re}\left[\zeta(i\lambda_I)\right]$ satisfies

$$\zeta_R'(\lambda_I) = \mathcal{C}_R'(\lambda_I) - \mathcal{F}_R'(\lambda_I) > 0 \quad \text{for all} \quad \lambda_I > 0 \,. \tag{6.5}$$

This leads to a key result that the path $\zeta(\Gamma_{I_+})$ can only intersect the imaginary axis exactly one or zero times. The only remaining issue will be to determine whether any such intersection point occurs on the positive or negative imaginary axis.

6.2 Above Competition Instability Threshold $D_{j,2} > D^*_{j,2}$; A Unique Unstable Real eigenvalue

Suppose that $b < 3 - 3/(2a)$ so that $\mathcal{C}_R(0) = \mathcal{C}(0) > 1/2$. Recall from (**??**) that this implies that $D_{j,2} > D^*_{j,2}$, and so we are above the competition instability threshold.

Since $F_R(0) = 1/2$, it follows that the endpoint of the path is at $\zeta(0) = \mathcal{C}_R(0) - \mathcal{F}_R(0) > 0$. Then, since the path $\zeta(\Gamma_{I_+})$ begins "at positive infinity" in the imaginary axis, stays within the right half-plane and ends at the positive real axis, owing to the key monotonicity property (6.5), it follows that we must have $[\arg\zeta]\,|_{\Gamma_{I_+}} = -\frac{\pi}{2}$. Therefore, we conclude from (**??**) that

$$N = 3/2 + \frac{1}{\pi}(-\frac{\pi}{2}) = 1 \quad \text{for all} \quad \tilde{\tau_j} > 0\,.$$

Our main conclusion regarding stability for the regime $D_{j,2} > D^*_{j,2}$ is that for any $j = 1, \ldots, K-1$, a K-hotspot steady-state solution is unstable due to a unique positive real eigenvalue that occurs for any $\tilde{\tau_j} > 0$.

6.3 Below Competition Instability Threshold $D_{j,2} < D^*_{j,2}$

Now suppose that $b > 3 - 3/(2a)$, so that $\mathcal{C}_R(0) = \mathcal{C}(0) < 1/2$. From (**??**) this means that $D_{j,2} < D^*_{j,2}$ and so we are below the competition instability threshold.

For this case, since $\zeta(0) = \mathcal{C}_R(0) - \mathcal{F}_R(0) < 0$, while $\mathcal{C}'_R(\lambda_I) > 0$ for any $\lambda_I > 0$ and $\mathcal{F}_R(\lambda_I) = 1/2$ at $\lambda_I = 0$ but decreases monotonically to 0 as $\lambda_I \to \infty$ (by Conjecture 4.4), there must be a unique root λ^*_I to $\zeta_R(\lambda^*_I) = 0$. Since $\zeta_I(0) = 0$, the endpoint is on the negative real axis, with exactly one crossing at $\lambda_I = \lambda^*_I$ when traveling from $\lambda_I = +\infty$. It is then clear that there are two distinctly different cases:

(I) If the crossing occurs on the positive imaginary axis, i.e. $\zeta_I(\lambda^*_I) > 0$, then $[\arg\zeta]\,|_{\Gamma_{I_+}} = \pi/2$, and so $N = 2$.

(II) If the crossing occurs on the negative imaginary axis, i.e. $\zeta_I(\lambda^*_I) < 0$, then $[\arg\zeta]\,|_{\Gamma_{I_+}} = -3\pi/2$, and so $N = 0$.

These two distinguishing cases were presented in Fig. 12, where we also noticed that case (I) and (II) implies that the curve approaches $\zeta(0) < 0$ as $\lambda_I \to 0^+$ in an anticlockwise and clockwise direction, respectively, with respect to the origin. Therefore, the final key step in the analysis is to distinguish path (I) from path (II).

We first establish that when $b > 3$ we obtain path (II) if either $\tilde{\tau_j} \gg 1$ or $\tilde{\tau_j} \ll 1$. Recall that $b > 3$ means $9\chi_{0,j}/2 > 3$, or equivalently

$$\frac{1}{\chi_{0,j}} < \frac{3}{2}\,.$$

This is precisely the condition (**??**) which was applied to (**??**) to show that the eigenvalues are stable regardless of $\tilde{\tau_j}$ in the $q = 3$ explicitly solvable case. This condition (**??**) implies a lower threshold

$$D_{j,2} < D^*_{j,2,\min} < D^*_{j,2}\,, \qquad D_{j,2,\min} = \frac{\omega^3}{4\pi^2 K^3}\,,$$

which for $q = 3$ case guarantees stability regardless of $\tilde{\tau_j}$. However, in the general case $q \neq 3$, the lack of an explicit form for $\mathcal{F}(\lambda)$ prevents us from obtaining the same conclusion as easily. We must then appeal to the local and far-field asymptotic properties of $\mathcal{C}$ and $\mathcal{F}$.

Firstly, if $\tilde{\tau_j} \gg 1$, we obtain from (6.3a) that

$$\mathcal{C}_R(\lambda_I) \sim a\left[\tilde{\tau_j} b - \frac{(3b)(3\tilde{\tau_j})}{9 + \lambda_I^2}\right] = \frac{a\tilde{\tau_j} b \lambda_I^2}{9 + \lambda_I^2}\,.$$

Then, upon setting $\mathcal{C}_R(\lambda_I) = \mathcal{F}_R(\lambda_I)$ and using $\mathcal{F}_R(0) = 1/2$, we obtain that $\zeta_R(\lambda_I) = 0$ has a root with $\lambda_I = \mathcal{O}(\tilde{\tau}^{-1/2})$ when $\tilde{\tau} \gg 1$. In particular, if we write $\lambda_I^* = \lambda_{I,0}^* \tilde{\tau_j}^{-1/2}$ so that $\lambda_{I,0}^* = \mathcal{O}(1)$, then we see that $ab\left(\lambda_{I,0}^*\right)^2/9 \sim 1/2$, which yields

$$\lambda_{I,0}^* \sim \frac{1}{\sqrt{ab}} \frac{3}{\sqrt{2}} .$$

Therefore, $\zeta_R(\lambda_I^*) = 0$ has a unique root when $\tilde{\tau_j} \gg 1$, and that this root is located near the the origin with asymptotics

$$\lambda_I^* \sim \frac{3}{\sqrt{2ab}} \tilde{\tau_j}^{-1/2} . \tag{6.6}$$

Now since $\mathcal{C}_I(\lambda_I) < 0$ on the range $0 < \lambda_I < \sqrt{3(b-3) + b/\tilde{\tau_j}} \sim \sqrt{3(b-3)}$ for $\tilde{\tau_j} \gg 1$, we have $\mathcal{C}_I(\lambda_I^*) < 0$ and so $\zeta_I(\lambda_I^*) < 0$. We then conclude that the crossing occurs on the negative imaginary axis as stipulated, which yields path (II).

Next, if we instead consider $\tilde{\tau_j} \ll 1$, then we have from (6.3a) that

$$\mathcal{C}_R(\lambda_I) \sim a\left[1 - \frac{3b}{9 + \lambda_I^2}\right] = a\left[\frac{3(3-b) + \lambda_I^2}{9 + \lambda_I^2}\right] , \tag{6.7}$$

which is independent of $\tilde{\tau_j}$. Thus, the intersection point where $\mathcal{C}_R = \mathcal{F}_R$ must occur at some $\lambda_I^* = \mathcal{O}(1)$. However, since $\mathcal{C}_I(\lambda_I) < 0$ on $0 < \lambda_I < \sqrt{3(b-3) + b/\tilde{\tau_j}} = \mathcal{O}(\tilde{\tau_j}^{-1/2})$ as $\tilde{\tau_j} \to 0$, which is now asymptotically large as $\tilde{\tau_j} \to 0$, we conclude that $0 < \lambda_I^* = \mathcal{O}(1) \ll \sqrt{3(b-3) + b/\tilde{\tau_j}}$. It follows that $\zeta_I(\lambda_I^*) < 0$, and so the crossing occurs on the negative imaginary axis as well. This again yields path (II).

In both cases, since the point $\zeta_I(\lambda_I^*) < 0$ is the only place the curve $\zeta(\Gamma_{I_+})$ crosses the imaginary axis, we have path (II) so that $N = 0$ by the formula (**??**). As a consequence, there are no unstable eigenvalues of the NLEP.

The remaining issue is to consider whether the statement above regarding N is still true *for any* $\tilde{\tau_j} > 0$ for the general case $q > 1$. We now consider three possible strategies for exploring this question.

One way to begin an analysis is to observe that $\mathcal{F}_R$ is independent of $\tilde{\tau_j}$ and that

$$\mathcal{C}_R(\lambda_I^*) - \mathcal{F}_R(\lambda_I^*) = 0 , \tag{6.8}$$

gives us an implicit relation for λ_I^* as a function of $\tilde{\tau_j}$. If we differentiate (6.8) with respect to $\tilde{\tau_j}$ we get

$$\frac{\partial}{\partial \lambda_I^*}\mathcal{C}_R(\lambda_I^*)\frac{d\lambda_I^*}{d\tilde{\tau_j}} + \frac{\partial}{\partial \tilde{\tau_j}}\mathcal{C}_R(\lambda_I^*) - \frac{\partial}{\partial \lambda_I^*}\mathcal{F}_R(\lambda_I^*)\frac{d\lambda_I^*}{d\tilde{\tau_j}} = 0 .$$

By letting $(\dots)'$ denote derivatives with respect to λ_I^*, and by using (6.3a), we obtain that

$$\left[\mathcal{C}_R'(\lambda_I^*) - \mathcal{F}_R'(\lambda_I^*)\right]\frac{d\lambda_I^*}{d\tilde{\tau_j}} = -\frac{\partial}{\partial \tilde{\tau_j}}\mathcal{C}_R(\lambda_I^*) = -ab\left(1 - \frac{9}{9 + \lambda_I^2}\right) . \tag{6.9}$$

Since $\mathcal{C}_R'(\lambda_I^*) > 0$ and $\mathcal{F}_R'(\lambda_I^*) < 0$ by (6.3a) and Conjecture (4.4), the expression above yields that

$$\frac{d\lambda_I^*}{d\tilde{\tau_j}} < 0 , \qquad \text{for all} \quad \tilde{\tau_j} .$$

Next, we observe that the upper end point of the interval of negativity of $\mathcal{C}_I(\lambda_I)$ is a function of $\tilde{\tau_j}$ as well. We will denote this endpoint as $h(\tilde{\tau_j})$. It satisfies

$$\frac{dh}{d\tilde{\tau_j}} \equiv \frac{d}{d\tilde{\tau_j}}\sqrt{3(b-3) + b/\tilde{\tau_j}} = -\frac{b}{2\tilde{\tau_j}^2\sqrt{3(b-3) + b/\tilde{\tau_j}}} < 0 .$$

In this way, we would conclude that the root λ_I^* stays within the interval $(0, h(\tilde{\tau_j}))$ if we can prove that the following inequality holds for all $\tilde{\tau_j} > 0$:

$$\frac{d\lambda_I^*}{d\tilde{\tau_j}} < \frac{dh}{d\tilde{\tau_j}} . \tag{6.10}$$

Then, since $\lambda_I^*(\tilde{\tau}_j) \in (0, h(\tilde{\tau}_j))$ has been shown above to be true for $\tilde{\tau}_j \ll 1$, the inequality above would imply that

$$\lambda_I^*(\tilde{\tau}_j) \in (0, h(\tilde{\tau}_j)) \quad \text{for all} \quad \tilde{\tau}_j > 0\,.$$

However, it seems analytically intractable to prove that (6.10) holds.

A second route of resolution would be to explore this issue numerically. For instance, in Fig. 14 we fix $\mathcal{D}_0 = 0.4$ so that $b \approx 3.1279 > 3$. Then, we find the unique root to $\zeta_R(\lambda_I) = 0$ for each τ_u from 0 to a large number to determine the range of possible λ_I values so that the eigenvalue is on the imaginary axis. Then, we compute $\zeta_I(\lambda_I)$ for λ_I on this range to determine its sign. For $q = 2$, where the NLEP is not explicitly solvable, we are able to confirm that $\zeta_I(\lambda_I) < 0$. Therefore, since path (II) applies, we conclude that the steady-state spike pattern is linearly stable for this parameter configuration. Nonetheless, it is still desirable to provide an analytical proof to show that the eigenvalues are in $\mathrm{Re}(\lambda) < 0$ for all choices of $q > 1$ and $0 < \tau_u < \infty$.

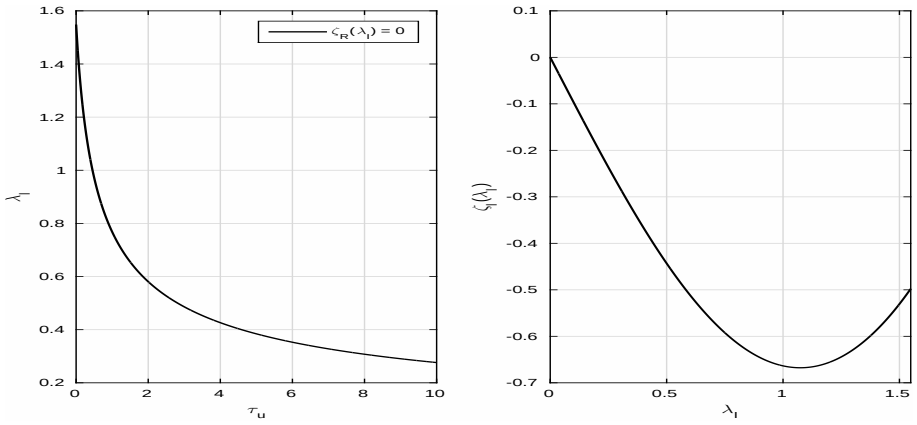

Figure 14: Numerical verification of a Nyquist path that predicts stability. Left: a plot of the unique roots to $\zeta_R(\lambda_I) = 0$ as τ_u varies. For very large τ_u, λ_I can be quite close to zero. Right: a plot of the possible range of values of $\zeta_I(\lambda_I)$ when the Nyquist contour hits the imaginary axis, where λ_I was chosen to vary from zero to the maximum value plotted on the left. The model parameters chosen were $\mathcal{D}_0 = 0.4$ and the parameters specified in (6.1).

The final route that we pursue to resolve this final case where $D_{j,2} < D^*_{j,2,\min}$ $(b > 3)$ is to assume an extra condition, as we will derive below. We first observe that $\mathcal{C}_R(\lambda_I) = 0$ at $\lambda_I = \lambda_{I_R} \equiv \sqrt{\frac{3(b-3)}{1+\tilde{\tau}_j b}}$, and we recall that $\mathcal{C}_I(\lambda_I) = 0$ at $\lambda_I = \lambda_{I_I} = \sqrt{(3(b-3) + b/\tilde{\tau}_j}$. Then, since $b/\tilde{\tau}_j > 1/(1 + \tilde{\tau}_j b)$ for $b > 1$, it follows that the inequality

$$\lambda_{I_R} < \lambda_{I_I}\,,$$

holds, because we have $b > 3$. For a typical picture of this scenario, we refer to Fig. 15 where we present full numerical computations for a particular parameter set.

We now determine the value λ_{I_M} for which $\mathcal{C}_R(\lambda_{I_M}) = 1/2$. We conclude that the root λ_I^* to $\zeta_R(\lambda_I) = 0$ must occur in $\lambda_{I_R} < \lambda_I^* < \lambda_{I_M}$. If we can further show that $\lambda_{I_M} < \lambda_{I_I}$, so that $\mathcal{C}_I(\lambda_{I_M}) < 0$, it follows also that $\mathcal{C}_I(\lambda_I^*) < 0$. This would imply that $\zeta_I(\lambda_I^*) < 0$ and $N = 0$. Therefore, the desired order of these special values of λ_I, which will guarantee that path (II) holds and so $N = 0$, is that

$$\lambda_{I_R} < \lambda_I^* < \lambda_{I_M} < \lambda_{I_I}\,. \tag{6.11}$$

For a particular set of parameter values this is illustrated in the numerical results shown in Fig. 16 .

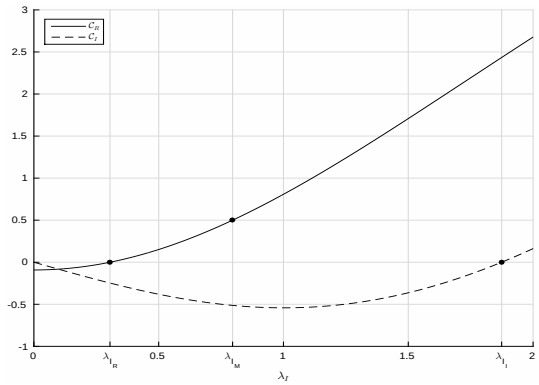

Figure 15: Locations of the three special points λ_{I_R}, λ_{I_I} and λ_{I_M} on the graphs of $\mathcal{C}_R$ and $\mathcal{C}_I$ versus λ_I, as discussed in the text. The model parameter values $\tau_u = 1$ and $\mathcal{D}_0 = 0.4$, together with those stated in (6.1), were used. The value $b \approx 3.1279 > 3$ was also numerically confirmed.

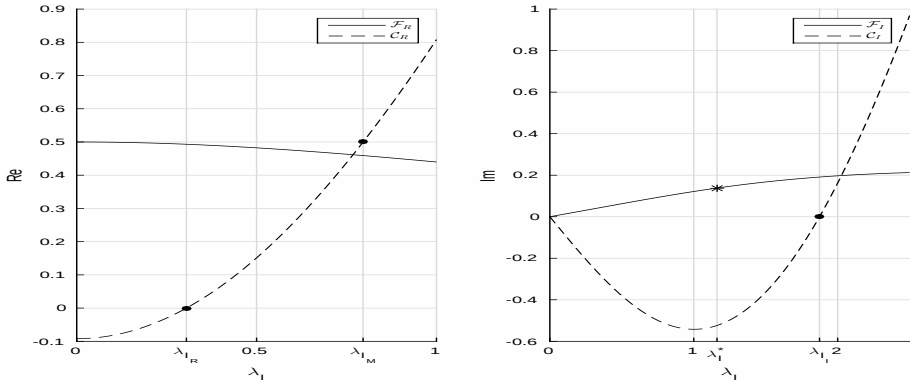

Figure 16: Numerical results for the location of λ_I^* (indicated by a star) relative to λ_{I_R}, λ_{I_M}, and λ_{I_I} (indicated by heavy dots), as stated in (6.11). The model parameters, $\tau_u = 1$ and $\mathcal{D}_0 = 0.4$, together with the parameter values stated in (6.1), were used.

We now show that the ordering (6.11) does in fact hold under an additional assumption. To show this, we consider the real part of (6.3a), and solve

$$\mathcal{C}_R(\lambda_{I_M}) = \frac{1}{2} = a\left[1 + \tilde{\tau}_j b - \frac{3b}{9+\lambda_{I_M}^2}\,(1+3\tilde{\tau}_j)\right].$$

This readily yields, after a little algebra, that

$$\frac{b(1+3\tilde{\tau}_j)}{9+\lambda_{I_M}^2} = \frac{1}{3}\left(1 + \tilde{\tau}_j b - \frac{1}{2a}\right) \quad \text{if} \quad 1 + \tilde{\tau}_j b - 1/(2a) > 0\,.$$

Next, we consider the imaginary part of (6.3a). Upon substituting the expression above into it, we calculate that

$$C_I(\lambda_{I_M}) = a\lambda_{I_M}\left[\tilde{\tau}_j - \frac{3b\tilde{\tau}_j + b}{9+\lambda_{I_M}^2}\right] = a\lambda_{I_M}\left[\frac{1}{3}(1 + \tilde{\tau}_j b - \frac{1}{2a})\right].$$

This expression can be written as

$$\mathcal{C}_I(\lambda_{I_M}) = -\frac{a}{3}\lambda_{I_M}\left[\tilde{\tau}_j(b-3) + \left(1 - \frac{1}{2a}\right)\right].$$

From this last expression, we conclude that if $b > 3$ and the *extra condition* $a > 1/2$ holds, then λ_{I_M} exists and $\mathcal{C}_I(\lambda_{I_M}) < 0$. It follows that $N = 0$ since $\mathcal{C}_I(\lambda_I^*) < \mathcal{C}_I(\lambda_{I_M}) < 0$, and then $\zeta_I(\lambda_I^*) < 0$ because $\mathcal{F}_I > 0$.

We summarize this result in the following statement:

Proposition 6.1 *Suppose that*

$$D_{j,2} < D_{j,2,\min}^* = \frac{\omega^3}{4\pi^2 K^3} \qquad \textit{(i.e. } b > 3\textit{)},$$

and that

$$\frac{\omega}{qU_0\chi_{0,j}} > \frac{1}{2} \qquad \textit{(i.e. } a > \tfrac{1}{2}\textit{)},$$

or equivalently,

$$D_{j,2} > \left(\frac{qU_0}{2\omega} - 1\right)\left(\frac{\omega^3}{2\pi^2 K^3}\right). \tag{6.12}$$

Then we have three different possibilities:

(I) If $\frac{qU_0}{2\omega} - 1 < 0$, *i.e.* $qU_0 < 2\omega = 2(U_{0,\max} - U_0)$, *or equivalently*

$$\omega = S(\gamma - \alpha) - U_0(1 + q/2) > U_0 q/2\,, \tag{6.13}$$

then the lower bound is negative and the inequality (6.12) is automatically true. Therefore, (6.13) together with $D_{j,2,} < D_{j,2,\min}^*$ *implies* $N = 0$ *and thus stability, or:*

(II) If $\frac{qU_0}{2\omega} - 1 > 1/2$, *then this conflicts with* $D_{j,2} < D_{2,j\,\min}^*$ *and no conclusion regarding stability can be made, or:*

(III) If $0 < \frac{qU_0}{2\omega} - 1 < 1/2$, *then if*

$$\left(\frac{qU_0}{2\omega} - 1\right)\left(\frac{\omega^3}{2\pi^2 K^3}\right) < D_{j,2} < D_{j,2,\min}^*\,,$$

we have $N = 0$ *for all* $\tilde{\tau} > 0$. *This gap condition holds with an analogous gap condition in* U_0.

$$U_0 q/3 < \omega = S\,[\gamma - \alpha] - U_0 < U_0 q/2\,.$$

It is an open problem to close the gap and drop the condition (6.12), and prove that $N = 0$ for all $\tilde{\tau}_j > 0$ and $0 < D_{j,2} < D_{j,2,\min}^*$, in agreement with what we discovered for the special case $q = 3$. However, Remark **??** also suggests that the threshold $D_{j,2,\min}^*$ could possibly be revised, as it may depend on q.

6.4 A Gap Between the Lower and Upper Thresholds: $D_{j,2,\min} < D_{j,2} < D_{j,2}^*$, Existence of Hopf Bifurcation

Having considered $D_{j,2}$ above $D_{j,2}^*$, where there is instability due to one unstable eigenvalue, and below $D_{j,2,\min}^*$, where we have stability subject to the extra condition, we now consider the gap region defined by

$$D_{j,2,\min}^* < D_{j,2} < D_{j,2}^* \,.$$

In this gap region we will argue that a Hopf bifurcation exists with respect to the parameter $\tilde{\tau}_j$. An example of a such a Hopf bifurcation point is illustrated in Fig. 17.

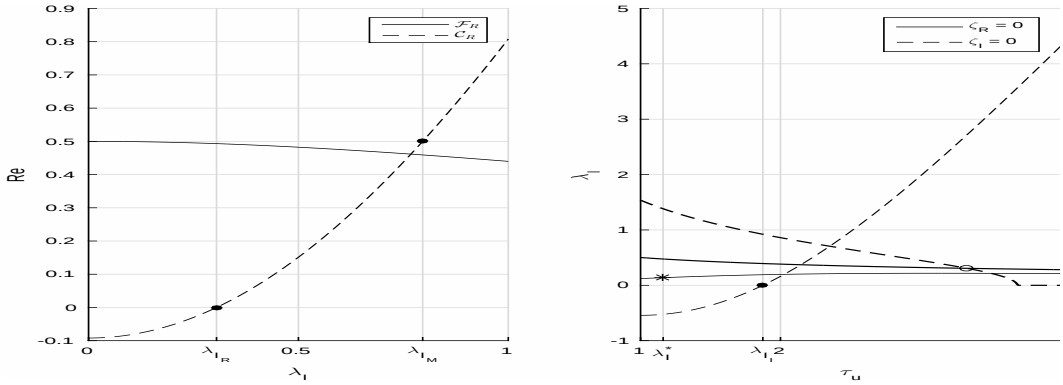

Figure 17: Locating the Hopf bifurcation point. The two curves shows the locus of the roots of $\zeta_R(\lambda_I)$ and $\zeta_I(\lambda_I)$ as functions of τ_u. Hopf bifurcation is determined numerically to occur at $\tau_u \approx 3.33$ and $\lambda_I \approx 0.307$, at the intersection of these two curves. The model parameters are $\mathcal{D}_0 = 0.6$ and those stated in (6.1). For this parameter set we confirm numerically that $3 - 3/(2a) \approx 2.397 < b \approx 2.714 < 3$, which satisfies (6.14).

Unlike in the explicitly solvable case, $q = 3$, where a Hopf bifurcation point can be located by a closed-form formula $\tilde{\tau}_j = \tilde{\tau}_{j,\text{Hopf}} = \mathcal{O}(1)$ using (**??**) (but only the mode $j = K - 1$ will actually occur), corresponding to the critical case $\zeta_I(\lambda_I^*) = 0$ (and by definition $\zeta_R(\lambda_I^*) = 0$ as well, so $\lambda = \pm i\lambda_I^*$ are a pair of purely imaginary eigenvalues corresponding to Hopf bifurcation), we seek only to confirm that if $\tilde{\tau}_j \ll 1$, we have path (II), i.e. stability, while if $\tilde{\tau}_j \gg 1$, then we have path (I), i.e. instability.

We first observe that when

$$3 - \frac{3}{2a} < b < 3 \,, \tag{6.14}$$

then $D_{j,2}$ is on the gap range

$$D_{j,2,\min}^* < D_{j,2} < D_{j,2}^* \,.$$

For the typical model parameter set given in (6.1) with two hotspots, these bounds are

$$0.4559 \approx \mathcal{D}_{0,\min}^* < \mathcal{D}_0 < \mathcal{D}_0^* \approx 0.7599 \,.$$

Since purely imaginary eigenvalue implies $\lambda = \pm i\lambda_I^*$, we still seek to find λ_I^* such that $\zeta_R(\lambda_I^*) = \zeta_I(\lambda_I^*) = 0$ directly. In other words, we are seeking the boundary case where the image of the positive imaginary axis is neither away from nor enclosing the origin, but exactly crosses through the origin.

Now on the range $\tilde{\tau}_j > \frac{b}{3(3-b)} > 0$, we have $\mathcal{C}_I(\lambda_I) > 0$ for all $\lambda_I > 0$. We can again let $\tilde{\tau}_j \to \infty$, as in the derivation of (6.6), to conclude that $\zeta_R(\lambda_I^*) = 0$ when

$$\lambda_I^* \sim \frac{3}{\sqrt{2ab}} \tilde{\tau}_j^{-1/2} \ll 1 \,.$$

Next, by using $\lambda_I^* = \mathcal{O}(\tilde{\tau}_j^{-1/2})$, together with $\mathcal{C}_I(\lambda_I^*)$ from (6.3a), we estimate that

$$\mathcal{C}_I(\lambda_I^*) \sim \frac{a\tilde{\tau}_j^{-1/2}}{9}\left[3\tilde{\tau}_j(3-b) + \mathcal{O}(1)\right] \sim \frac{a\tilde{\tau}_j^{1/2}}{9}(3-b) > 0\,,$$

since $b < 3$. Then, since $\mathcal{C}_I(\lambda_I^*) = \mathcal{O}(\tilde{\tau}_j^{1/2}) \gg 1$, but $\mathcal{F}_I(\lambda_I^*) = \mathcal{O}(\tilde{\tau}_j^{-1/2})$ when $\lambda_I^* = \mathcal{O}(\tilde{\tau}_j^{-1/2})$, we conclude that $\zeta_I(\lambda_I^*) > 0$ as $\tilde{\tau}_j \to +\infty$. This implies that path (I) holds and $N = 2$.

On the other hand, when $\tilde{\tau}_j \to 0^+$ we can repeat a previous calculation given in (6.7) to obtain that the intersection of $\mathcal{C}_R(\lambda_I)$ and $\mathcal{F}_R(\lambda_I)$ must occur at some $\lambda_I^* = \mathcal{O}(1) > 0$. Then, since for $\tilde{\tau}_j \to 0$ we have from (6.3a) that $\mathcal{C}_I(\lambda_I^*) < 0$ because $b > 0$, we must conclude that $\zeta_I(\lambda_I^*) < 0$ when $\tilde{\tau}_j \ll 1$. This implies that in the limit $\tilde{\tau}_j \ll 1$, path (II) holds and $N = 0$.

We then prove the existence of a Hopf bifurcation by appealing to a continuous path argument, namely that $\lambda_I^* = \lambda_I^*(\tilde{\tau}_j)$ as a continuous function. Since $N = 0$ for $\tilde{\tau}_j \ll 1$, while $N = 2$ for $\tilde{\tau}_j \ll 1$, there must exist a *minimum value* of $\tilde{\tau}_{j,\mathrm{H}opf} > 0$ such that $\zeta_I(\lambda_I^*(\tilde{\tau}_{j,\mathrm{H}opf})) = 0$ exactly with $\lambda_I^* > 0$. However, it is not clear whether there are other values of $\tilde{\tau}_j$ at which other Hopf bifurcations occur for $\tilde{\tau}_j > \tilde{\tau}_{j,\mathrm{H}opf} > 0$.

One way to attempt to prove uniqueness of the Hopf bifurcation value would be to prove a condition of one-way traversality at the onset of a purely imaginary eigenvalue. To do so, we may again let $\lambda = \lambda_R + i\lambda_I$ and consider both real part and imaginary part as a function of $\tilde{\tau}_j$, so that the Hopf bifurcation occurs at $\lambda_I(\tilde{\tau}_j) = \lambda_I^*$ where $\lambda_R = 0$. If one can further show that $d\lambda_R/d\tilde{\tau}_j > 0$ whenever we have a root on the imaginary axis, it would follow that the locus of any eigenvalue in the complex plane can cross the imaginary axis only once, and in only the direction from left to right. It appears to be analytically rather difficult to prove such a one-way transversal crossing condition.

6.5 Conclusions on the Stability of a Symmetric $K-$Hotspot Steady-State

For $q = 2, 3, 4$, suppose that Conjecture 4.4 holds and that $K \geq 2$. Let N denote the number of eigenvalues with positive real part. Then, for any mode of competition instability $j = 1, \ldots, K-1$, we have established the following statement:

(i) If $D_{j,2} > D_{j,2}^*$, then $N = 1$ for all $\tilde{\tau}_j > 0$. The steady-state K-spike pattern is unstable for any q.

(ii) If $D_{j,2,\min}^* < D_{j,2,} < D_{j,2}^*$, then there exists a Hopf bifurcation threshold $\tilde{\tau}_H$ which is possibly non-unique when $q \neq 3$. Moreover, we have $N = 2$ when $\tilde{\tau}_j \gg 1$, and hence instability. Otherwise if $\tilde{\tau}_j \ll 1$, then we have $N = 0$, and hence stability. When $q = 3$, the threshold $\tilde{\tau}_H$ is unique with formula given in (**??**), and we have $N = 0$ and $N = 2$ for $\tilde{\tau}_j$ below and above the threshold $\tilde{\tau}_H$, respectively.

(iii) If $D_{j,2} < D_{j,2,\min}^*$, then for $q \neq 3$ we have $N = 0$ if $\tilde{\tau}_j \gg 1$ and $\tilde{\tau}_j \ll 1$. If we suppose further the additional condition that $\omega = S(\gamma - \alpha) - U_0 > U_0 q/2$, then we have $N = 0$ for any $\tilde{\tau}_j > 0$. For $q = 3$, we have that $N = 0$ for any $\tilde{\tau}_j > 0$ with no extra condition needed.

Remark 6.2

1. *A reason for considering integral values of q only in the range* $\{2, 3, 4\}$ *is that we assumed in the course of deriving the NLEP* **??** *that* $\tau_u \ll \mathcal{O}(\epsilon^{-2})$ *(see the calculations leading to 3.15). Then, for the parameter*

$$\tilde{\tau}_j = \tau_u \mathcal{O}(\epsilon^{q-3})\,,$$

to be $\mathcal{O}(1)$, we must have that $\tau_u = \mathcal{O}(\epsilon^{3-q})$. This establishes that $q < 5$ is required to satisfy the assumption that $\tau_u \ll \mathcal{O}(\epsilon^{-2})$. If $q = 5$, then the ODE for the perturbation η at (3.16a) will be changed to

$$\mathcal{D}_0 \alpha^q \eta_{xx} = \epsilon^2 \tau_u \lambda \alpha^q \eta \,,$$

where $\tau_u = \mathcal{O}(\epsilon^{-2})$. This will result in a different problem to be solved for $\eta(x)$, and consequently a different value for $\eta(0)$. Ultimately, this leads to a different NLEP that requires a separate analysis.

2. *Conjecture (4.4) is rigorously established in the literature except for the statement $\mathcal{F}_R'(\lambda_I) < 0$ for $q = 4$. However, this monotonicity condition for $q = 4$ was readily established numerically in Fig. 2.*

6.6 Asymptotic Determination of Hopf Bifurcation Threshold

Finally, we would like to see if we can determine λ_I^* and $\tilde{\tau}_{j,\mathrm{H}opf}$ asymptotically as $b \to 3$ from below. We recall that for the explicitly solvable case $q = 3$ that we have $\tilde{\tau}_{j,\mathrm{H}opf} \to \infty$ as $b \to 3^-$ ($D_{j,2} \to \left(D^*_{j,2,\min}\right)^-$) and, correspondingly, that $\lambda_{I,H} \to 0^+$. This motivates us to consider the general case $q \neq 3$ to examine whether only the known local behavior of $\mathcal{C}_R$, $\mathcal{C}_I$, $\mathcal{F}_R$, and $\mathcal{F}_I$ as $\lambda_I \to 0$, is involved in estimate the Hopf bifurcation point.

From [34], it is well known for any $q > 1$ that

$$\mathcal{F}_R(\lambda_I) \sim \frac{1}{2} - k_c \lambda_I^2 + \cdots \,, \qquad \mathcal{F}_I(\lambda_I) \sim \frac{\lambda_I}{4}\,(1 - 1/q) \quad \text{as} \quad \lambda_I \to 0\,,$$

where $k_c > 0$ is a constant depending on q. We then recall that $\mathcal{C}_R(\lambda_I)$ can be written as

$$\mathcal{C}_R(\lambda_I) = \frac{a}{9 + \lambda_I^2}\left[3(3-b) + (1 + \tilde{\tau}_j b)\lambda_I^2\right] .$$

To examine the region near $b = 3$, we introducing a detuning parameter δ by $\delta = 3 - b$, where $0 < \delta \ll 1$. We then look for a root to $\mathcal{C}_R(\lambda_I) = \mathcal{F}_R(\lambda_I)$ near $\lambda_I = 0$ when $\tilde{\tau}_j \gg 1$. To this end, we expand $\mathcal{C}_R(\lambda_I)$ near $\lambda_I = 0$ as

$$\mathcal{C}_R(\lambda_I) = \frac{a}{9 + \lambda_I^2}\left[3\delta + (1 + 3\tilde{\tau}_j)\lambda_I^2 + \mathcal{O}(\tilde{\tau}_j \delta \lambda_I^2)\right] .$$

This suggests that we must have the dominant balance $\tilde{\tau}_j \lambda_I^2 = \mathcal{O}(1)$ so that $\mathcal{C}_R \to 1/2 = \mathcal{F}_R(0)$ as $\lambda_I \to 0$. This motivates the introduction of the rescaling

$$\lambda_I \sim \tilde{\tau}_j^{-1/2} \lambda_{I,0}\,,$$

which must be chosen in such a way that

$$\frac{a}{9}\left[3\lambda_{I,0}^2 + \mathcal{O}(\delta)\right] \sim \frac{1}{2}\,.$$

This yields that

$$\lambda_{I,0} = \sqrt{\frac{3}{2a}}\,.$$

Therefore, for $\tilde{\tau}_j \gg 1$ and $b = 3 - \delta$ with $0 < \delta \ll 1$, the unique root of $\zeta_R(\lambda_I) = 0$ is located asymptotically at

$$\lambda_I \sim \sqrt{\frac{3}{2a}}\,\tilde{\tau}_j^{-1/2}\,.$$

Next, we relate $\tilde{\tau}_j$ to δ by enforcing that $\mathcal{C}_I(\lambda_I) \sim \mathcal{F}_I(\lambda_I)$ as $\lambda_I \to 0^+$. This latter condition yields that

$$a\lambda_I\left(\frac{3\tilde{\tau}_j\delta - 3 + \mathcal{O}(\delta) + \tilde{\tau}_j\lambda_I^2}{9 + \lambda_I^2}\right) \sim \frac{\lambda_I}{4}\,(1 - 1/q)\,.$$

Upon cancelling λ_I from both sides of this expression, and putting $\tilde{\tau}_j\lambda_I^2 = 3/(2a)$, we get

$$\frac{a}{9}\left[3\tilde{\tau}_j\delta - 3 + \frac{3}{2a}\right] = \frac{1}{4}(1-1/q)\,.$$

Upon solving this equation for $\tilde{\tau}_j$, we get

$$\tilde{\tau}_j \sim \delta^{-1}\left(1 + \frac{1}{4a} - \frac{3}{4aq}\right)\,.$$

In summary, provided that

$$1 + \frac{1}{4a}(1-3/q) > 0\,, \tag{6.15}$$

we have that as $b \to 3^-$, the Hopf bifurcation occurs at

$$\tilde{\tau}_j = \tilde{\tau}_{j,\mathrm{H}opf} \sim \frac{1}{\delta}\left(1 + \frac{1}{4a}\,(1-3/q)\right)\,, \tag{6.16}$$

with corresponding frequency

$$\lambda_I^* \sim \delta^{1/2}\sqrt{\frac{3}{2a}}\left(1 + \frac{1}{4a}\,(1-3/q)\right)^{-1/2}\,, \tag{6.17}$$

where $\delta = 3 - b \to 0^+$.

Finally, let us compare this result for general q to the explicit result that we obtained earlier for the exactly solvable case $q = 3$.

Firstly, we observe that the quadratic equation (**??**) for λ that occurs when $q = 3$ is equivalent to

$$\lambda^2 + \left(\frac{1 + \tilde{\tau}_j(b-3)}{\tilde{\tau}_j}\right)\lambda + \frac{[b - 3 + 3/(2a)]}{\tilde{\tau}_j} = 0\,.$$

We conclude that a Hopf bifurcation occurs if the coefficient of λ vanishes, i.e. if $\tilde{\tau}_{j,\mathrm{H}opf} = (3-b)^{-1} = \delta^{-1}$ in agreement with setting $q = 3$ in (6.16). In addition, since at the Hopf bifurcation we have

$$(\lambda_I^*)^2 = \frac{b - 3 + 3/(2a)}{\tilde{\tau}_j} = \frac{1}{\tilde{\tau}_j}\left(\frac{3}{2a} - \delta\right)\,,$$

we conclude that

$$\lambda_I^* \sim \delta^{1/2}\sqrt{\frac{3}{2a}}\,.$$

This expression agrees with (6.17) upon setting $q = 3$.

When $q = 4$, we readily observe that the assumption (6.15) for (6.16) and (6.17) is always satisfied. However for $q = 2$, we have to require that $a > 1/8$ in order for (6.15) to hold. This means for $a = \omega/(U_0\chi_{0,j})$, $b = 9\chi_{0,j}/2 = 3$, which gives $\chi_{0,j} = 2/3$, that we must have the condition

$$a = \frac{\omega}{\frac{4}{3}U_0} > \frac{1}{8}\,,$$

which is equivalent to the requirement that $\omega > U_0/6$. Therefore, we conclude that a Hopf bifurcation occurs when $D_{j,2} \to (D_{j,2,\min})^+$ with asymptotics given by (6.16) and (6.17) if the condition

$$\omega = S(\gamma - \alpha) - U_0 > U_0/6\,, \tag{6.18}$$

holds. In other words, the asymptotic conclusions hold provided we are not too close to the existence threshold $\omega = 0$ of the hotspot pattern.

Remark 6.3 *The fact that, for $q = 2$, the Hopf bifurcation with the asymptotics (6.16) and (6.17) does not occur for*

$$0 < S(\gamma - \alpha) - U_0 < U_0/6\,,$$

when $b \to 3^-$, i.e. as $D_{j,2} \to \left(D^*_{j,2,\min}\right)^+$ does not contradict the fact that there exists a Hopf bifurcation when

$$D^*_{j,2,\min} < D_{j,2} < D^*_{j,2}\,.$$

It only shows that the limiting asymptotics is not of the form where $\tilde{\tau}_j \to \infty$ and $D_{j,2} \to \left(D^*_{j,2,\min}\right)^+$ simultaneously.

7 Discussion

In this chapter we used the method of matched asymptotic expansions to construct a steady-state hotspot solution to (1.6) having K hotspots of a common amplitude in the limit $\epsilon \to 0$ for the regime $D = \mathcal{O}(\epsilon^{-2})$. We then studied the spectrum characterizing the linear stability properties of this steady-state solution by analyzing an NLEP with two nonlocal terms. We studied the NLEP by first considering a special case with patrol focus degree $q = 3$, which results in an explicitly solvable NLEP and, consequently, an explicit formula for the principal eigenvalue. Explicitly solvable NLEP problems also appear in [14, 19, 20]. The general case was then studied using the argument principle to count the number of unstable eigenvalues in the right half plane. This procedure was first developed to study the stability of steady-state spike patterns for the Gierer-Meinhardt model (cf. [34]) and now has a rather large body of literature (see [14] and the references therein). Our conclusions from the explicitly solvable case $q = 3$ are considerably stronger than those for the non-explicitly solvable case $q \neq 3$. In particular, when $q = 3$, two thresholds $\mathcal{D}_{0,lower}$ and $\mathcal{D}_{0,upper}$ given in (**??**) were determined so that the a multiple-hotspot pattern is stable when $\mathcal{D}_0 < \mathcal{D}_{0,lower}$ and unstable due to a competition instability when $\mathcal{D}_0 > \mathcal{D}_{0,upper}$. Moreover, an explicit formula for the existence of Hopf bifurcation $\tau_u = \tau_{Hopf}$ when $\mathcal{D}_{0,lower} < \mathcal{D}_0 < \mathcal{D}_{0,upper}$ was given in (**??**). In contrast to the absence of a Hopf bifurcation for the basic crime model with no police intervention, as discovered in [14], the window of existence for a Hopf bifurcation given by $(\mathcal{D}_{0,lower}, \mathcal{D}_{0,upper})$ vanishes exactly when $U_0 = 0$. In other words, the third component of the PDE system (1.6), modeling the police interaction, is essential to inducing the possibility of oscillations. Moreover, unlike the case of the Gray-Scott and Gierer-Meinhardt models studied in [16] and [34], where synchronous oscillatory instabilities of the spike amplitudes robustly occur and are the dominant instability, our three-component system exhibits asynchronous oscillatory instabilities. These asynchronous, anti-phase, oscillations of the spike amplitudes have the qualitative interpretation that, for a range of police diffusivities, the police presence is only able to mitigate the amplitude of certain hotspots at the expense of the growth of other hotspots in different spatial regions.

However, when $q \neq 3$, we had difficulty in analytically proving results as strong as for the case $q = 3$. In particular, we were not able to prove, without assuming further conditions, that a multiple hotspot pattern is stable when the rescaled criminal diffusivity $\mathcal{D}_0$ is below the same lower threshold defined earlier in the $q = 3$ case. One possibility is that the definition of the lower threshold should be revised and should change with q. When $\mathcal{D}_0$ is between the lower and upper thresholds, we were able to prove the existence of a Hopf bifurcation, but we cannot show uniqueness of the critical Hopf bifurcation value in τ_u. These are interesting open problems that warrant further study. Most importantly, we would like to investigate what are the mathematical relationships between the explicitly solvable case $q = 3$ and the non-explicitly solvable case $q \neq 3$, so that the strong results from the explicitly solvable case can potentially carry over to the general case.

7.1 Open Problems and Future Directions

With regards to our police model, with simple police interaction, studied in this chapter, it would be interesting to consider the more challenging $D = \mathcal{O}(1)$ regime. One key question would be to investigate whether the police presence can eliminate the peak insertion behavior that was found for the basic crime model to lead to the nucleation of new spikes of criminal activity. In this direction it would be interesting to determine the influence of the police presence on the global bifurcation of multiple hotspot steady-state solutions.

This suggests that there should also be discrete spectra of the full problem that are near zero as $\epsilon \to 0$. These are the "small" eigenvalues that are related to translational instabilities. Our analysis of the NLEP characterizes only those eigenvalues that are $\mathcal{O}(1)$ as $\epsilon \to 0$, which can lead to $\mathcal{O}(1)$ time-scale instabilities.

A second interesting direction would be to study the effect of police presence on crime patterns when the police interaction is modeled by the predator-prey dynamics case $I(U, \rho) = U\rho$. Preliminary results suggest that the NLEP will now have three nonlocal terms, which makes a detailed stability analysis very challenging. However, the determination of the competition instability threshold, corresponding to the zero eigenvalue crossing, should be readily amenable to analysis.

A third direction would be to consider spatial patterns in more than a simple 1-D spatial context. In this context, it would be interesting to extend the 2-D stability results in [14] for the basic crime model, to study the existence of stability of crime hotspots in 2-D domains in the presence of police. In particular, we would like to investigate the stability and dynamics of 2-D hotspots, allowing for either of our two different models of police intervention.

A Deriving the Continuum Limit

Acknowledgments

M. J. Ward was supported by the NSERC Discovery Grant 81541. We gratefully acknowledge helpful discussions with Theodore Kolokolnikov and Juncheng Wei on the NLEP analysis.

References

[1] H. Berestycki, J.-P. Nadal, *Self-organised critical hot spots of criminal activity*, Europ. J. Appl. Math., **21**(4-5), (2010), pp. 371–399.

[2] H. Berestycki, J. Wei, M. Winter, *Existence of symmetric and asymmetric spikes for a crime hotspot model*, SIAM J. Math. Anal., **46**(1), (2014), pp. 691–719.

[3] P. L. Brantingham, P. J. Brantingham, *Crime patterns*, McMillan, (1987).

[4] R. Cantrell, C. Cosner, R. Manasevich, *Global bifurcation of solutions for crime modeling equations*, SIAM J. Math. Anal., **44**(3), (2012), pp. 1340–1358.

[5] Discover, Science for the Curious (2010), [Fight Crime with Mathematics ranks in Top 100 Stories in 2010]. Retrieved from http://discovermagazine.com/2011/jan-feb/60.

[6] A. Doelman, R. A. Gardner, T. J. Kaper, *Large stable pulse solutions in reaction-diffusion equations*, Indiana U. Math. J., **50**(1), (2001), pp. 443–507.

[7] A. Doelman, H. van der Ploeg, *Homoclinic stripe patterns*, SIAM J. Appl. Dyn. Systems, **1**(1), (2002), pp. 65-104.

[8] M. R. D'Orsogna, M. Perc, *Statistical physics of crime: A review*, Physics of Life Reviews, **12**, (2015), pp. 1-21

[9] Y. Gu, Q. Wang, G. Yi, *Stationary patterns and their selection mechanism of urban crime models with heterogeneous near-repeat victimization effect*, Europ. J. Appl. Math., **28**(1), (2017), pp. 141–178.

[10] D. Iron, M. J. Ward, J. Wei, *The stability of spike solutions to the one-dimensional Gierer-Meinhardt model*, Physica D, **150**(1-2), (2001), pp. 25–62.

[11] S. Johnson, K. Bower, *Domestic burglary repeats and space-time clusters: The dimensions of risk*, Europ. J. of Criminology, **2**, (2005), pp. 67–92.

[12] P. A. Jones, P. J. Brantingham, L. Chayes, *Statistical models of criminal behavior: The effect of law enforcement actions*, Math. Models. Meth. Appl. Sci., **20**, Suppl., (2010), pp. 1397–1423.

[13] T. Kolokolnikov, M. J. Ward, J. Wei, *The existence and stability of spike equilibria in the one-dimensional Gray-Scott model: The low feed-rate regime*, Studies in Appl. Math., **115**(1), (2005), pp. 21–71.

[14] T. Kolokolnikov, M. J. Ward, J. Wei, *The stability of steady-state hot-spot patterns for a reaction-diffusion model of urban crime*, DCDS-B, **19**(5), (2014), p. 1373–1410.

[15] R. McKay, T. Kolokolnikov, *Stability transitions and dynamics of localized patterns near the shadow limit of reaction-diffusion systems*, DCDS-B, **17**(1), (2012) pp. 191–220.

[16] T. Kolokolnikov, M. J. Ward, J. Wei, *The existence and stability of spike equilibria in the one-dimensional Gray-Scott model: The low feed rate regime*, Studies in Appl. Math, **115**(1), (2005), pp. 21–71.

[17] T. Kolokolnikov, J. Wei, *Stability of spiky solutions in a competition model with cross-diffusion*, SIAM J. Appl. Math., **71**, (2011), pp. 1428–1457.

[18] D. J. B. Lloyd, H. O'Farrell, *On localised hotspots of an urban crime model*, Physica D, **253**, (2013), pp. 23–39.

[19] I. Moyles, W.-H. Tse, M. J. Ward, *Explicitly solvable nonlocal eigenvalue problems and the stability of localized stripes in reaction-diffusion systems*, Studies in Appl. Math., **136**(1), (2016), pp. 89–136.

[20] Y. Nec, M. J. Ward, *An explicitly solvable nonlocal eigenvalue problem and the stability of a spike for a class of reaction-diffusion system with sub-diffusion*, Math. Model. of Nat. Phenom., **8**(2), (2013), pp. 55–87.

[21] K. Painter, T. Hillen, *Spatio-temporal chaos in a chemotaxis model*, Physica D, **240**, (2011), pp. 363–375.

[22] H. van der Ploeg, A. Doelman, *Stability of spatially periodic pulse patterns in a class of singularly perturbed reaction-diffusion equations*, Indiana Univ. Math. J., **54**(5), (2005), pp. 1219–1301

[23] A. B. Pitcher, *Adding police to a mathematical model of burglary*, Europ. J. Appl. Math., **21**(4-5), (2010), pp. 401–419.

[24] J. D. M. Rademacher, *First and second order semi-strong interaction in reaction-diffusion systems*, SIAM J. Appl. Dyn. Syst., **12**(1), (2013), pp. 175–203.

[25] RAIDS Online, *Crime density maps for West Vancouver, B.C., Canada and Santa Clara-Sunnyville, California, US*, BAIR Analytics, (2015), Inc. Retrieved from http://raidsonline.com/.

[26] L. Ricketson, *A continuum model of residential burglary incorporating law enforcement*, unpublished, (2011). Retrieved from http://cims.nyu.edu/~lfr224/writeup.pdf.

[27] N. Rodriguez, A. Bertozzi, *Local existence and uniqueness of solutions to a PDE model for criminal behavior*, M3AS (special issue on Mathematics and Complexity in Human and Life Sciences), **20**(1), (2010), pp. 1425–1457.

[28] I. Rozada, S. Ruuth, M. J. Ward, *The stability of localized spot patterns for the Brusselator on the sphere*, SIAM J. Appl. Dyn. Sys., **13**(1), (2014), pp. 564–627.

[29] M. B. Short, M. R. D'Orsogna, V. B. Pasour, G. E. Tita, P. J. Brantingham, A. L. Bertozzi, L. B. Chayes, *A statistical model of criminal behavior*, Math. Models. Meth. Appl. Sci., **18**, Suppl., (2008), pp. 1249–1267.

[30] M. B. Short, A. L. Bertozzi, P. J. Brantingham *Nonlinear patterns in urban crime - hotspots, bifurcations, and suppression*, SIAM J. Appl. Dyn. Sys., **9**(2), (2010), pp. 462–483.

[31] M. B. Short, P. J. Brantingham, A. L. Bertozzi, G. E. Tita (2010), *Dissipation and displacement of hotpsots in reaction-diffusion models of crime*, Proc. Nat. Acad. Sci., **107**(9), pp. 3961-3965.

[32] W. Sun, M. J. Ward, R. Russell, *The slow dynamics of two-spike solutions for the Gray-Scott and Gierer-Meinhardt systems: competition and oscillatory instabilities*, SIAM J. Appl. Dyn. Syst., **4**(4), (2005), pp. 904–953.

[33] W.-H. Tse, M. J. Ward, *Hotspot formation and dynamics for a continuum model of urban crime*, Europ. J. Appl. Math., **27**(3), (2016), pp. 583–624.

[34] M. J. Ward, J. Wei, *Hopf bifurcations and oscillatory instabilities of spike solutions for the one-dimensional Gierer-Meinhardt model*, J. Nonlinear Sci., **13**(2), (2003), pp. 209–264.

[35] J. Wei, *On single interior spike solutions of the Gierer–Meinhardt system: uniqueness and spectrum estimates*, Europ. J. Appl. Math., **10**(4), (1999), pp. 353–378.

[36] J. Wei, *Existence and stability of spikes for the Gierer-Meinhardt system*, book chapter in *Handbook of Differential Equations, Stationary Partial Differential Equations*, Vol. 5 (M. Chipot ed.), Elsevier, (2008), pp. 489–581.

[37] J. Q. Wilson, G. L. Kelling, *Broken windows and police and neighborhood safety*, Atlantic Mon., **249**, (1998), pp. 29–38.

[38] J. R. Zipkin, M. B. Short, A. L. Bertozzi, *Cops on the dots in a mathematical model of urban crime and police response*, DCDS-B, **19**(5), (2014), pp. 1479–1506.